



HAL
open science

Quaternary sedimentary processes on the Bahamas: From platform to abyss

K. Fauquembergue, E. Ducassou, T. Mulder, J.J.G. Reijmer, J. Borgomano,
A. Recouvreur, V. Hanquiez, C. Betzler, M. Principaud, L. Chabaud, et al.

► **To cite this version:**

K. Fauquembergue, E. Ducassou, T. Mulder, J.J.G. Reijmer, J. Borgomano, et al.. Quaternary sedimentary processes on the Bahamas: From platform to abyss. *Marine Geology*, 2023, 459, pp.107044. 10.1016/j.margeo.2023.107044 . hal-04254858

HAL Id: hal-04254858

<https://hal.science/hal-04254858>

Submitted on 23 Oct 2023

HAL is a multi-disciplinary open access archive for the deposit and dissemination of scientific research documents, whether they are published or not. The documents may come from teaching and research institutions in France or abroad, or from public or private research centers.

L'archive ouverte pluridisciplinaire **HAL**, est destinée au dépôt et à la diffusion de documents scientifiques de niveau recherche, publiés ou non, émanant des établissements d'enseignement et de recherche français ou étrangers, des laboratoires publics ou privés.

Quaternary sedimentary processes on the Bahamas: From platform to abyss

K. Fauquembergue ^{a,*}, E. Ducassou ^a, T. Mulder ^a, J.J.G. Reijmer ^b, J. Borgomano ^{c,e}, A. Recouvreur ^a, V. Hanquiez ^a, C. Betzler ^f, M. Principaud ^a, L. Chabaud ^a, N. Fabregas ^a, J. Giraudeau ^a, V. Bout-Roumazelles ^d, P. Moal-Darrigade ^a, M.-C. Perello ^a, E. Poli ^e

^a Univ. Bordeaux, CNRS, Bordeaux INP, EPOC, UMR 5805, F-33600 Pessac, France

^b Vrije Universiteit Amsterdam, Faculty of Science, Department of Geosciences, De Boelelaan 1085, 1081 HV Amsterdam, the Netherlands

^c Observatoire des Sciences de l'Univers (OSU) Institut Pythéas, Centre National de la Recherche Scientifique (CNRS) (Joint Research Unit [UMR] 7330), Institut de Recherche pour le Développement (IRD) (UMR 161), Collège de France – USC INRA, Centre Européen de Recherche et d'Enseignement de Géosciences de l'Environnement (CEREGE), Aix-Marseille Université, Marseille, France

^d Laboratoire d'Océanologie et de Géosciences, UMR 8157 Univ Lille–CNRS-ULCO-IRD, bâtiment SN5, 59655 Villeneuve d'Ascq cedex, France

^e Projet “Carbonates”, Exploration & Production SCR/RD, Total S.A., CSTJF, Avenue Larribau, Pau 64000, France

^f Universität Hamburg, Institut für Geologie, 20146 Hamburg, Germany

Keywords:

Carbonate

Slope

Bahamas

Quaternary

Leeward vs. Windward Sediment processes

Abstract

Understanding the interaction between sediment production on and export from shallow-water areas of platforms and slopes is primordial when assessing sedimentary processes on a carbonate-platform scale. In this manuscript we explore variations in facies, sediment export, sediment deposition and reorganisation, hydro-acoustic- and small-scale sedimentary structures, but also assess the variability in current systems as observed during the Quaternary for the north-facing margin of Little Bahama Bank (LBB) and compare those characteristics with features observed on other slopes surrounding LBB and Great Bahama Bank (GBB).

Over the past decade, the northern margin of LBB was explored during a series of oceanographic cruises of the CARAMBAR project, which included the collection of 24.270 km² of bathymetry data, 6.398 km of very high-resolution seismic profiles, and 42 cores covering water depths ranging from 177 m to 4873 m. This study evaluates the results obtained from the analysis of sediment cores retrieved in the Great Abaco Canyon area (GAC), located between the lower northern LBB slope, which is connected to the abyssal plain. The analysis of the shallower parts of the LBB slope relies on earlier studies and are complementary to our data, and allow for a detailed analysis of the sedimentary processes acting along the entire LBB slope.

The data reveal that Quaternary sediment distribution differs when moving from the north-eastern to the north-western LBB slope. The entire LBB slope is dissected by numerous canyons. Gravity processes enriched in coarse platform components occur infrequently and are concentrated within lobes in the east. Only coarse-grained rich bank facies can concentrate

coarse grains on this margin. The western LBB slope is mostly influenced by fine-grained platform export and current circulation. The deeper GAC area is dominated by pelagic sediments that are supplied from the canyon sides and through tributaries. The sediment composition confirms that pelagic sediment production and current movements determine the sediment-deposition and redistribution processes at this site.

The comparison with other Bahamian slopes demonstrates that a leeward position agrees with high sedimentation rates on the slopes resulting in specific morphologic structures, such as gullies and sediment waves, related to fine-grained sediment export, whereas platform-derived coarse-grained facies are deposited down-stream in larger structures, such as canyons, that are not affected by the main wind direction. Slope angle could also have an impact on grain-size export, as it appears that coarse-grained deposits are frequent on steep slopes like those bordering the Exuma Sound basin.

1. Introduction

At present a large series of major sedimentary systems can be found around the world that are exclusively composed of carbonate sediments, e.g., the Bahamas, the Maldives, the Mascarene Plateau (Indian Ocean). Carbonate factories in these settings reflect carbonate sediment production linked to strict environmental conditions such as water temperature, light conditions, and nutrient availability (Schlager, 2003; Michel et al., 2018; Reijmer, 2021). This combination of environmental parameters enables prolific sediment production and significant export of shallow-water skeletal and non-skeletal platform sediments to deeper slopes and basins. A clear and accurate understanding of the mechanisms driving the export of these sediments, coarse to fine, to the deep seafloor is essential to assess the overall depositional processes and the reservoir aspect of these deposits. Previous studies have highlighted that the efficiency of sediment export for all grain-size fractions depends on factors such as platform morphology and the presence of reefs, e.g. Puga-Bernabéu et al. (2011, 2013, 2014) for the mixed Great Barrier Reef system and Etienne et al. (2021) for the Lansdowne Bank (SW Pacific Ocean), or dominant wind direction interacting along the platform margin that may support or restrain the export of sediments (Schlager and Ginsburg, 1981; Tournadour, 2015).

At the Bahamas, passing winter fronts and daily processes mainly determine sediment export out of the shallow-water realms (e.g., Wilber et al., 1990; Wilson and Roberts, 1992, 1995; Hickey et al., 2000; Roth and Reijmer, 2004, 2005; Principaud et al., 2018). Hurricanes are often highlighted as main sediment export events, but have only reduced impact on sedimentation patterns on the platform (Rankey et al., 2004; Reeder and Rankey, 2009) as they mainly stir up muds in the shallow carbonate platform realm. Hence, indirectly they facilitate the export of fine sediment through continuous processes like tidal and ocean currents. Preferential sediment export is illustrated by the progradation-aggradation geometries visible in seismic profiles of Great Bahama Bank (Eberli and Ginsburg, 1987, 1989). These profiles demonstrate a leeward-margin dominated closing of intraplatform seaways and westward progradation of the Cenozoic Great Bahama Bank margin. Other leeward and windward margin sedimentation processes were detailed through ODP Leg 101 (Austin Jr. et al., 1986) and IODP Leg 166 (Swart et al., 2000) studies.

Slope morphologies vary throughout the Bahamas depending on the interaction between sediment export, tides, platform margin morphology i.e., presence or absence of shoals or islands, as well as shallow- and deep-water ocean currents (e.g., Wilber et al., 1990; Harwood and Towers, 1988; Rankey and Doolittle, 2012; Betzler et al., 2014). Variations in the grain-

size spectrum of the exported sediment (Rendle-Bühning and Reijmer, 2005), and their quantity related to eustatic sea-level variations ('highstand shedding'; Droxler et al., 1983; Schlager et al., 1994) together with in-situ submarine (Grammer et al., 1993) and microbial binding of the upper slopes (Reolid et al., 2017), as well as terrestrial cementation (Dravis, 1996) and karst processes during exposure of the shallow-water carbonate platform (e.g. Labourdette et al., 2007; Rankey and Doolittle, 2012) determine the sedimentation processes on the slope and the ultimate morphology of the platform margin and slope itself.

The upper slopes along the Bahamas are marked by a very steep cliff-like upper slope with a series of terraces (Wilber et al., 1990; Grammer et al., 1993; Rankey and Doolittle, 2012; Mulder et al., 2012). The middle slope displays varying angles of repose and slope adjustment processes related to the sediment composition (Harwood and Towers, 1988; Kenter, 1990), combined with slope channels (Mulder et al., 2012; Tournadour et al., 2017), Mass Transport Deposits (MTD; Tournadour et al., 2015; Wunsch et al., 2017; Le Goff et al., 2020) and sediment sorting processes related to deep-water currents (Betzler et al., 2014). Latter processes also relate to the development of a series of contourite deposits bordering Great Bahama Bank and Little Bahama Bank (Bergman, 2005; Eberli and Betzler, 2019; Mulder et al., 2019).

All in all, the Quaternary slopes of the Bahamian slopes offer the opportunity to investigate the interaction between oceanic processes and platform sediment production/export at a regional scale. The Bahamian archipelago is made up of >700 islands that occur dispersed along extensive carbonate platforms on which the maximum water depth does not exceed 20 m (Fig. 1). Sediment production on these platforms itself and its export towards the associated slope deposits has been discussed extensively over the last few decades, focusing on stratigraphic architectures and platform-to-slope transition and physiography (Playton et al., 2010; Betzler et al., 2014; Reijmer et al., 2015a, 2015b; Chabaud et al., 2015; Wunsch et al., 2017; Mulder et al., 2017).

This study focuses on analysing sedimentation patterns observed in cores obtained from the Great Abaco Canyon positioned on the northern Bahamian slope of Little Bama Bank (LBB), the northernmost platform of the Bahamian archipelago. A comparison of the sedimentation history in this area with existing sedimentological and seismic data will be made to generate a detailed assessment of slope sedimentation patterns on this carbonate margin to (i) assess the factors controlling the skeletal and non-skeletal sediment transfer from the shallow-water platform to the adjacent slope and basin during the Quaternary (Fig. 1); (ii) evaluate sediment production, export, deposition and redistribution of both fine- and coarse-grained deposits; and (iii) finally make a comparison with other platform slopes of the Bahamas to appraise the variations for leeward (e.g., western GBB) and windward (e.g., LBB) orientated slopes.

2. Geological and Oceanographic setting

2.1. Geological setting

The Great Abaco Canyon (GAC) runs more or less parallel to the northern margin and the northern slope of the LBB (Fig. 1). It actually marks a regional structural boundary between the Bahamas and the Blake Plateau and can be linked to the Great Abaco Fracture Zone that dates back to pre-Santonian time (Mullins et al., 1982). Vertical movement along this fracture zone during the Upper Cretaceous to Eocene are related to the Cuban orogenesis and probably resulted in the formation of the early Great Abaco Canyon. Another expression of the kinematic

evolution of the Cuban fold and thrust belt within the associated Bahamian foreland is the Santaren Anticline (Masferro et al., 1999, 2002). This NW-SE trending fold runs parallel to other folds and thrusts observed onshore and offshore of Cuba and displays fold growth between the latest Mid-Eocene to Pliocene and possibly even at present (Masferro et al., 1999). Over time the Great Abaco Channel environment experienced a series of events with partial infill (Austin Jr et al., 1988) during the Paleogene succeeded by increased sediment transport towards the Blake-Bahama Basin during the Oligocene to Middle Miocene (Benson and Sheridan, 1975; Mullins et al., 1982; Bliefnick et al., 1983; Austin Jr et al., 1988). Finally, GAC acted as transport channel for the redeposition of sediments derived from the Blake Bahama Ridge as well as sediment that originated from LBB (Mulder et al., 2012; Tournadour et al., 2017; Fauquembergue et al., 2018; Recouvreur et al., 2020).

2.2. Sediment export from platforms to slopes and climate control

During periods of falling sea level and sea-level lowstands, active cementation occurs on the platforms (Schlager et al., 1994; Dravis, 1996; Kievman, 1998) and karstification affects previously formed highstand deposits (Myroie and Carew, 1995; Ford and Williams, 2007). When the platforms are subsequently flooded, the water mass that cover the platform will be subjected to seasonal variations in temperature, and associated changes in salinity, wind patterns, tides, and fluctuations in nutrient and carbonate saturation levels. Platform flooding is the first-order prerequisite controlling platform-top sediment production and subsequent sediment export of tropical carbonate platforms (Schlager et al., 1994; Jorry et al., 2020; Paul et al., 2012). In the Bahamas, where platforms water depth does not exceed 20 m, this scenario occurred only during 17% of the last 400 kyr (Fig. 2; Bintanja et al., 2005). Sediment export during these high sea-level conditions is called “highstand shedding” (Droxler and Schlager, 1985; Schlager et al., 1994).

Wilson and Roberts (1992, 1995) and Hickey et al. (2000) demonstrated that turbid waters are exported from the platform to the Bahamian slopes during passing winter cold fronts. Cold fronts can last between five and seven days and affect the Florida surroundings between 15 and 25 times per winter (Hardy and Henderson, 2003). During cold fronts, the atmosphere chills the water masses on the shallow carbonate bank, which densify and subsequently flow off-bank forced by tidal currents (Hickey et al., 2000). After cold fronts have move away, the atmosphere warms and evaporation increases leading to a higher water mass salinity, which maintains the off-bank flow. This mechanism, recognized as the source of most off-bank export, is called “density cascading” (Wilber et al., 1990; Wilson and Roberts, 1992, 1995; Chabaud et al., 2015; Fauquembergue, 2018; Eberli and Betzler, 2019). Depending on their trajectories, hurricanes can also induce conditions for platform sediment remobilization and export to deep-water settings. In the Bahamas, hurricane frequency varies and may occur up to three times per year during summer (Cry, 1965; Park, 2012). Evidence of sediment export after hurricanes have been highlighted by aerial photography and satellite images (Perkins and Enos, 1968; Major et al., 1996; Rankey et al., 2004; Reeder and Rankey, 2008; Fauquembergue et al., 2018) and also by the sedimentological record on platforms and slopes (Boss and Neumann, 1993; Shinn et al., 1993; Major et al., 1996; Rankey et al., 2004; Reeder and Rankey, 2009; Park et al., 2009; Toomey et al., 2013; Fauquembergue et al., 2018). Tidal flushing can also export turbid water generated by hurricanes towards the slopes (Mulder et al., 2017; Fauquembergue et al., 2018). However, two hurricanes with similar strength and trajectory may induce different sediment export patterns and hence could produce different sedimentary archives (Perkins and Enos, 1968).

2.3. Bahamian slopes: Sediment transfer influenced by ocean currents and water masses

While sediment remobilization on the platforms is affected by meteorological and, more generally, climatological factors, slope morphologies from platform margins to abyssal plains are influenced by (i) tectonic processes, (ii) the distribution, amount and composition of platform sediment exported to the slopes, (iii) surface to deep ocean current circulation (Fig. 1), (iv) intensity of cementation, (v) microbial activity or (vi) the presence of biological constructions (Mullins and Neumann, 1979; Grammer et al., 1993; Reolid et al., 2017). Two ocean currents relate to the occurrence of drifts on the Bahamian slopes: the Antilles Current and the Florida Current (Fig. 1; Mullins et al., 1980; Meinen et al., 2004; Bergman, 2005; Meinen et al., 2019). The Antilles Current circulates as eddies (Fig. 1); it borders the Blake Bahama Escarpment (BBE) and merges with the Florida Current on the north-western edge of LBB to form the Gulf Stream (Fig. 1). These currents are counterbalanced by the southward flowing Deep Western Boundary Current (DWBC) that circulates along the deeper part of the BBE and contribute to drift development (below 2000 m depth; Fig. 1; Cartwright, 1985; Biló and Johns, 2020). The DWBC corresponds to the lower part of the North Atlantic Deep Water (NADW) in the deep Nares Abyssal Plain.

Platform derived sediments are enriched in aragonite, allowing their tracing in deep waters (Droxler, 1984). Currently, there is no consensus on the Aragonite Compensation Depth (ACD) around the Bahamas. Indeed, Balsam (1983) and Droxler et al. (1988a, 1988b) propose an ACD that deepens to >4100 m east of the Bahamas, James and Choquette (1983) propose this limit to be at about 2000 m. Carbonates, especially aragonite, are already partially dissolved at two water depths levels in the Florida Straits: 800–1000 m and below 1500 m (Schwarz and Rendle-Bühning, 2005).

2.4. Hydrodynamics

Wave energy resulting from swells and winds mostly hit the northern LBB from the northeast to the southwest (Fig. 1; Hine and Neumann, 1977; Rankey and Doolittle, 2012). This results in the development of a windward platform margin where shallow currents mostly move from the open ocean to the platform (Hine and Neumann, 1977). The wind direction influences carbonate sedimentation in two ways. Firstly, it influences the distribution of shallow-water platform facies, with fine-grained sediment concentrated in areas protected by shoals and islands (Fig. 1). Secondly, it determines the quantity of sediment exported to the slopes, with winds mainly driving sediment transport from the platform top down the slope along leeward margins, as platform-top sediment exported to slopes is limited along windward margins.

2.5. The windward northern LBB slope: Sedimentology and geomorphology

Seven main depositional areas with distinctive sedimentation patterns can be distinguished on the Bahamian slopes (Fig. 3) like along the LBB northern slope (Mullins et al., 1980; Chabaud et al., 2015; Tournadour, 2015; Tournadour et al., 2015; Chabaud, 2016; Tournadour et al., 2017; Recouvreur et al., 2020). The descriptive features of the LBB area are detailed in Fig. 4. They consist of: (1) the uppermost slope which includes four terraces and four escarpments that

gave rise to a Holocene, a few kilometres wide, sediment wedge. This wedge was only observed on the western uppermost slope; (2) the upper slope that extends to small canyon heads and landslides developed on (3) the middle slope; (4) the lower slope that is more extensive in the west and reduced in the east as the eastern area is dissected by the GAC head that incises (5) the Blake Plateau. The GAC canyon incises the (6) BBE and connects with the (7) Nares abyssal plain. The sedimentation patterns present on the LBB platform margin to basin transect can also be distinguished on other Bahamian slopes (Fig. 4).

The Holocene wedge located on the (1) northern LBB uppermost slope was fed by sediment produced on the four terraces that were shaped during stagnations in sea level (e.g., between meltwater pulses periods; Rankey and Doolittle, 2012; Mulder et al., 2017; Fauquembergue et al., 2018). The development of the oldest part of the wedge occurred before the flooding of the platform at 6 ka (Fauquembergue et al., 2018). Once the platform was reflooded, a strong increase in platform-derived sediment input to the slope was observed. Although some facies could be directly related to sediment export due to hurricane impact, sediment supply to the wedge mainly occurred by density cascading after the passage of cold fronts over the archipelago (Fauquembergue et al., 2018). The mean sedimentation rate for the entire wedge is ~ 1.25 m/kyr (Fauquembergue et al., 2018).

The (2) upper and (3) middle LBB slope domains are characterized by numerous small-sized canyons and a mass transport complex (MTC) that developed at the surface of the LBB drift (Mulder et al., 2012; Tournadour et al., 2015, 2017; Recouvreur et al., 2020). The morphology of the canyons displays an east-west variability (Fig. 4), which may be due to a regional tectonic tilting and/or the impact of processes related to the westward progression of the GAC head (Mulder et al., 2012; Recouvreur et al., 2020) combined with the increased influence of the LBB drift morphology moving westward (Fig. 4). Earlier studies highlighted the reduced influence of gravity processes in the north-western LBB slope but also stressed the impact of ocean circulation on the overall sedimentation pattern (Chabaud et al., 2015; Chabaud, 2016). The highest sedimentation rates, >15 cm/kyr (Chabaud et al., 2015; Chabaud, 2016), were measured during sea-level highstands, which agrees with the highstand shedding model of Schlager et al., (1994). In the eastern slope area, canyons are more prone to erosion than those present in the west (Fig. 4; Recouvreur et al., 2020).

The (4) lower slope morphology varies between the eastern and western slope. Distributary furrows leading to small depositional areas characterize the mouths of the western canyons (Fig. 4; Tournadour et al., 2015). The across-slope extension of the eastern lower slope is short (< 10 km) compared to the western slope and shows a rapid transition to the Blake Plateau (Fig. 4; Recouvreur et al., 2020). Contourite drift deposits cover the GAC northern side (Mulder et al., 2018; Recouvreur et al., 2020). However, the origin of the currents that shaped these deposits is under discussion with the Antilles Current or the DWBC as the most likely candidates (Recouvreur et al., 2020).

The (5) Blake Plateau is incised by two giant canyons that are orientated perpendicular to the (6) BBE and cross it: the Little Abaco Canyon (LAC) and the GAC (Fig. 4; Mulder et al., 2018; Recouvreur et al., 2020). Despite the fact that the GAC is three times longer than the LAC, both canyons share numerous similarities as they both are u-shaped and have steep morphologies with distinct plunge pools (Mulder et al., 2018; Recouvreur et al., 2020). Southward, two other giant canyons incise the BBE: the Great Bahama Canyon (GBC) and the Exuma Canyon (Figs. 1 and 4). Sedimentation at the (7) mouths of these canyons, on the Nares abyssal plain, is dominated by DWBC-derived clay supply that occurs interbedded with carbonate gravity deposits, especially in the coarse-grained deposits at the mouth of Exuma Canyon (Droxler, 1984; Cartwright, 1985; Ravenne et al., 1985; Ravenne, 2002).

At present, the slopes of the windward margin of LBB and the leeward margin of GBB display morphological similarities. Both include a Holocene sediment wedge, enclose mass transport deposits, and contain contourite drifts, but also display some differences such as the presence of a channel-levee system, and gullies that are only present on the GBB slope (Betzler et al., 2014; Principaud, 2016; Wunsch et al., 2017, 2018). For the Holocene sediment wedge on the western GBB slope (Wilber et al., 1990; Roth and Reijmer, 2004, 2005; Principaud, 2016) and on LBB density cascading is the main process supplying muds to the entire slope depositional environment as smaller-sized sediment plumes produced during hurricanes tend to have a more local impact (Perkins and Enos, 1968; Boss and Neumann, 1993). However, because the sedimentation rate is higher along the GBB margin (11 m/kyr; Wilson and Roberts, 1992; Roth and Reijmer, 2004) than for the northern LBB Holocene wedge with ~ 1.25 m/kyr (Fauquembergue et al., 2018). In addition, the downslope extent of the GBB wedge is further than for the LBB wedge; the GBB mud-prone sedimentary wedge distribution reaches over 10 km and the LBB wedge covers <3 km.

3. Material and methods

3.1. Oceanographic cruises

This study discusses and summarizes the results of sedimentological and stratigraphic analyses on sediment cores collected on the north-eastern LBB slope and GAC area during the CARAMBAR 2 - Leg 1 cruise (Mulder et al., 2018) with the R/V L'Atalante operated by Genavir (Fig. 4). To develop a regional model of sediment deposition during the Quaternary along the northern LBB, the results obtained will be combined with studies of sediment cores retrieved during two other cruises that were part of the CARAMBAR project (Fig. 4): (i) the R/V Le Suroît (Ifremer) CARAMBAR - Leg 2 (2010) cruise, north-western LBB slope (Mulder et al., 2012), and (ii) the R/V H.G. Walton Smith (University of Miami) CARAMBAR 1.5 (2014) cruise, north-western LBB uppermost slope.

3.2. Acoustic data

In this study, results obtained from the cores will be added to the previously published acoustic data that were acquired along the northern LBB, which are summarized in Table 1. A total of $\sim 21,000$ km² of multibeam echosounder bathymetry and reflectivity data, and ~ 8000 km of Very High Resolution (VHR) 2D seismic-reflection data were collected during the various marine campaigns to study the subsurface geometry of the deposits (Mulder et al., 2012, 2017, 2018; Tournadour, 2015; Recouvreur et al., 2020).

3.3. Sedimentation analysis

3.3.1. Cores database and stratigraphy

A total of 42 Küllenberg cores were used to develop the regional model, including 29 cores previously dated and analysed (Chabaud et al., 2015; Chabaud, 2016; Fauquembergue et al., 2018), and 13 cores collected during the CARAMBAR 2 - Leg 1 cruise (Mulder et al., 2018; GAC area and eastern slope) that were analysed for this study (Table 2; Fig. 5). Core lengths varied between 1 m and 12 m. The total core length spans ~225 m. Sedimentological analyses and interpretation of the CARAMBAR-Leg 2 (2010) and CARAMBAR 1.5 (2014) cores were presented in Chabaud et al. (2015), Chabaud (2016) and Fauquembergue (2018).

3.3.2. Facies analysis

Lithological descriptions are based upon visual descriptions, photographs and X-ray radiographs that were obtained using a Digital X-ray imaging system SCOPIX at the UMR EPOC of the CNRS-University of Bordeaux EPOC. Density differences present in the cores were analysed using the SCOPIX X-ray image-processing tool. Grain-size measurements were conducted on 2021 sediment samples using a laser particle size analyser (Malvern Mastersizer 2000). A 63 µm wet sieving was conducted on each sediment core at 40 cm resolution. The fine (smear slides) and coarse fractions were analysed under a reflected light binocular and an optical microscope, respectively, in order to qualify and quantify the grains and help to establish the stratigraphy.

Semi-quantitative analysis of major and minor chemical elements was carried out using an Avaatech XRF scanner (10 kV, 400 µA, 10 s, and 30 kV 2000 µA, 15 s) at the University of Bordeaux, which provides a downcore view of the elemental composition of the sediments. The normalized ratio (XRF counts of [Fe + Si + Ti + Al])/[total XRF counts], was used as a proxy for detrital input. As illite is a potassium- rich mineral, the normalized ratio “Kn” (XRF counts of K / total XRF counts), was used as a marker of potassium enrichment. The normalized ratio (XRF counts of Ca) / (total XRF counts), was also compared with the calcium content of selected samples (3 samples/core) by Bernard calcimeter measurements.

The combination of SCOPIX X-ray image-processing (Migeon et al., 1998), sediment composition, grain-size measurements, smear slides and XRF scanner (Croudace et al., 2006) data allowed to determine the sediment variations within the deposits, evaluate their internal structures and assess the sediment production sources.

3.3.3. Core stratigraphy

Three different methods were used to establish the stratigraphy within the 13 cores collected in the GAC area following the procedure developed by Chabaud et al. (2015) and Chabaud (2016).

The primary age model was based on the correlation between the $\delta^{18}\text{O}$ curve obtained on the planktonic foraminifer *Globigerinoides ruber albus* n.subsp. in core CAR2KS13 (Fig. 6) and variations within the LR04 stack (Lisiecki and Raymo, 2005) to estimate the limits of glacial and interglacial transitions and define the corresponding Marine Isotopic Stages (MIS).

Sediment packages rich in Sr are interpreted to represent periods with high platform-derived input (Droxler et al., 1988a, 1988b; Croudace et al., 2006). In the Bahamas, Sr can be used as a marker of glacials (depletion in Sr induced by low platform-derived productivity) and interglacials (enrichment in Sr induced by high platform-derived productivity; Droxler, 1984);

the ratio Sr/Ca was used to (i) establish correlations between the core CAR2KS13 and other cores but also (ii) to define the precise limits of MIS transitions in the cores.

This stratigraphic framework was constrained by biostratigraphic datums or biohorizons defined by the first and last occurrences of calcareous micro- and nannofossil species. Biostratigraphy is based on planktonic foraminifer assemblages (fraction >150 μm) and coccoliths (fraction <150 μm) biohorizons calibrated with the CAR2KS13 $\delta^{18}\text{O}$ curve (Fig. 6). For the fraction >150 μm , interglacials are characterized by the abundance of the *Globorotalia menardii* complex, *Pulleniatina obliquiloculata*, *Globorotalia tumida flexuosa* and *Globigerina ruber*. Glacial periods are characterized by the abundance of *Neogloboquadrina dutertrei* and *Globorotalia inflata*. For the fraction <63 μm , both the top of the most recent *Gephyrocapsa caribbeanica* acme zone and the first appearance of *Emiliana huxleyi* occur close to the MIS 8–9 boundary (Weaver, 1983; Pujos, 1988; Giraudeau et al., 1998).

4. Results

4.1. Stratigraphy and sedimentation rates of the GAC study area

Isotope stratigraphic results together with sedimentological data enabled us to accurately define the different MIS in the studied cores and calculate sedimentation rates for the individual glacial and interglacial intervals. Mean sedimentation rates are shown in Fig. 7. Locally, sedimentation rates can reach 5 cm/kyr (CAR2KS09 in GAC tributaries; Fig. 7) or locally even exceed 22 cm/kyr (CAR2KS11; Fig. 7). Cores located near turbidite systems have the highest sedimentation rates (Fig. 7). During glacial periods, sedimentation rates are 50% lower than those measured on average for the interglacial periods of the entire GAC area (2.6 cm/kyr vs 5.1 cm/kyr; Fig. 7). The highest sedimentation rates during glacial periods are estimated at the GAC head (~5 cm/kyr for CAR2KS05; Fig. 7) and at the GAC deep-water outlet (> 4 cm/kyr for CAR2KS14). Sedimentation rates in cores located close the GAC head (Figs. 5 and 7) and northern and southern GAC margins vary between 2 cm/kyr and 4 cm/kyr (Fig. 7). Despite these similarities, the GAC head area and the GAC northern margin seem to evolve differently than the GAC southern margin during glacial/interglacial cycles (Fig. 7). The southern margin presents large differences in sedimentation rates between glacial (~1 cm/kyr) and interglacial (~5 cm/kyr) phases unlike those for the GAC head (with ~3.3 cm/kyr during glacials and ~2.5 cm/kyr during interglacials), and those for the northern margin (with ~3 cm/kyr during glacials and ~2 cm/kyr during interglacials) that remain fairly stable.

Based on the extrapolation of the mean sedimentation rates in the cores as obtained from the individual core stratigraphies, an assessment can be made of the age intervals of the individual sedimentary bodies visible in the VHR profiles surrounding each core (e.g., Fig. 5 for CAR2KS13). This method, used in Fauquembergue et al. (2018), was initially developed for upper Quaternary sedimentary bodies. The method can only make an estimate of the start of overall sediment deposition for the study area. Two sediment bodies (sampled by core CAR2KS11 and core CAR2KS14) had no clear base layer and hence an estimate of their age at the base of the VHR profile could not be made. The oldest estimated age is found on the slide scar as sampled by core CAR2KS12 (2.3 Ma). All other bases of sedimentary bodies can be dated as Middle to Upper Pleistocene (Table 3).

Fig. 7. Sedimentation rates by MIS obtained on LBB studied cores, from western to eastern areas. Yellow intervals represent interglacials and blue intervals glacials. MIS stratigraphy and

ages shown on the right. MIS recorded at the base of the cores (dotted line) are assumed to be incomplete. (For interpretation of the references to colour in this figure legend, the reader is referred to the web version of this article.)

4.2. Sedimentological facies of GAC study area

Five sedimentary facies were recognized within the study area (Fig. 8):

- Facies 1 displays an overall high clay content (> 50%) with values of up to 80% clays, and is entirely composed of grains <2 μm . This facies occurs in dm-scale layers in cores that encompass MIS 7 and MIS 9 in the GAC area (CAR2KS01, CAR2KS02, CAR2KS04, CAR2KS12, CAR2KS13 and dominates in core CAR2KS14; Figs. 6, 9, 10 and 11). Except for core CAR2KS14, clay generally overlies a base of silty lamina lacking calcium carbonate with severely altered grains. The non-clay fraction (mainly carbonate mud rich in coccoliths) increases from sequence base to sequence top. Core CAR2KS14, located in the Nares abyssal plain at the mouth of the GAC (Fig. 9) is dominated by hemipelagic clay mixed with some aragonite needles.
- Facies 2 is the most common facies found in cores CAR2KS01, CAR2KS02, CAR2KS03, CAR2KS04, CAR2KS05, CAR2KS07, CAR2KS08, CAR2KS10, CAR2KS12, CAR2KS13. This facies is carbonate-rich with over 87% CaCO_3 , and corresponds to deep-sea pelagic wackestones lacking terrigenous material (as defined by Bates and Jackson, 1987, and Neuendorf et al., 2011). This facies comprises muds, < 2 μm grain-size range, and silts, the 2–63 μm fraction. Smear slide revealed that the clay fraction mainly consists of carbonate components; coccoliths >80%, calcite grains and aragonite needles <5% of sediment composition (Figs. 6, 9 and 10). The clay fraction is dominant before MIS 8 (> 60%; Figs. 9 and 10), and the silt fraction is dominant from MIS 8 up to recent times (>55%; Figs. 9 and 10). The silt fraction is dominated by pelagic grains; ~30% planktonic foraminifers, ~10% pteropods and ~ 20% pteropod fragments. Facies 2 shows <5% of undetermined, potentially detrital grains in the >2 μm fraction. The sand fraction consists of planktonic foraminifers, pteropods (generally >65% of the entire sample), as the fine fraction is mainly composed of coccoliths (> 90%). For interglacial periods, the input of aragonite needles in this facies increases slightly, but never exceeds 5%. The elemental ratios $(\text{Fe} + \text{Si} + \text{Ti} + \text{Al})_n$ and Kn presents similar patterns in this facies in all cores (Figs. 6, 9 and 10), with the exception of a few levels at Terminations I, II and III (e.g., in core CAR2KS13; Fig. 6) where the increase in $(\text{Fe} + \text{Si} + \text{Ti} + \text{Al})_n$ is generally greater than Kn .
- Facies 3 sediments correspond to grainstones, as they are depleted in mud but rich in pteropods, pteropod fragments and planktonic foraminifera in the sandy fraction (> 80%). The facies only occurs in core CAR2KS01 during MIS 6 and in core CAR2KS14 during MIS 1.
- Facies 4 sediments are rudstones and contain coarse elements with a strong diagenetic overprint (up to 74%) whose origin cannot be determined. The sediments also comprise up to 11% of platform-derived grains with *Cyclorbiculina compressa*, *Amphistegina* sp., *Clavulina nodosaria*, *Miniacina miniacea*, aggregated broken shells, *Halimeda* flakes; *Neoconorbina* sp., olividae gastropods, *Bigenenerina nodosaria*. This facies is present in a few cores located at the southern GAC margin that reached MIS 5 (e.g., cores CAR2KS02, CAR2KS03 and CAR2KS01) and in core CAR2KS11 positioned on the lobe at the mouth of one of the canyons (Fig. 11).
- Facies 5 shows up in two cores located on the levees of the GAC tributaries. The sediment composition of its coarser fraction is similar as can be found in facies 3, but fine-grained

elements allow to consider this facies as packstones. Laminations can be identified on X-rays images (Fig. 8). The two cores that recovered this facies (cores CAR2KS09 and CAR2KS10; Fig. 10) contain 0.03% and 0.06% radiolarians, respectively (*Lithocyclia angusta*, *Actinomma arcadophorum*, *Acrosphaera spinosa*, *Collosphaera huxleyi*). Radiolarians reach maximum values of 4% in core CAR2KS09 and 0.14% in core CAR2KS14.

4.3. Sedimentological facies defined in earlier studies

Four other facies were previously described for the northern LBB slope (Fig. 8; Chabaud et al., 2015; Chabaud, 2016; Fauquembergue et al., 2018) and consist of:

- Contouritic facies, was linked to current deposits (Chabaud, 2016). The fraction exceeding 150 μm is particularly rich in lithoclasts (> 20% instead of <1% in other facies composing cores CARKS24 and CARKS25; Fig. 5).
- The laminated platform-derived facies was found in the uppermost slope core CARGC09 (Fig. 5). This facies was interpreted to be deposited by a hurricane (Fauquembergue et al., 2018).
- The slightly cemented facies is related to low sedimentation rates over the northwestern LBB canyon interfluvies (cores CARKS26 and CARKS29; Fig. 5). It contains multiple centimetre-sized nodules resulting from the strong current and non-deposition between the canyon heads (Chabaud et al., 2015; Chabaud, 2016).
- Periplatform ooze is the most abundant facies present in the deposits of the north western LBB slope. It occurs in most cores collected along the upper and middle slope (Chabaud et al., 2015; Chabaud, 2016). This facies contains platform- and slope-derived grains in both the >150 μm fraction (Halimeda flakes, planktonic and benthic foraminifers) and the fine fraction (< 63 μm) that contains a mix of aragonite needles and coccoliths. Sediments present on the upper- most slope and the ones infilling the MTC topography (Fig. 3) are slightly enriched in platform-derived sands.

4.3.1. Facies interpretation

The final facies interpretation used combines the results from this GAC study and those from earlier LBB studies (Chabaud et al., 2015; Chabaud, 2016; Fauquembergue et al., 2018) is as follows (Fig. 8):

- Facies 1 is clay rich and contains some fine (coccoliths) and coarse (pteropods, planktic foraminifers) carbonate grains. It is interpreted as hemipelagic facies.
- Facies 2 contains the same elements as the hemipelagic facies, facies 1, but is depleted in clay. It is interpreted as pelagic facies.
- Facies 3 corresponds to facies “2” but is depleted in the fine fraction. It is interpreted as slope-derived coarse-grained facies.
- Facies 4 is interpreted as platform-derived coarse-grained facies.

- Facies 5 agrees with laminated slope derived grained facies.

4.4. Spatial distribution exported sediments

Platform-derived grains are exported as both coarse and (mostly) fine grains. A limited amount of platform-derived sands was present within the Holocene wedge on the western uppermost slope (Fig. 12). The sand occurs together with a large amount of fine fraction sediments that are rich in aragonite needles, and actually form the main component of the periplatform ooze wackestones. Deposits filling the MTC slide scar (Fig. 12) are similar to the Holocene wedge deposits but their fine fraction is enriched in coccoliths. In contrast, the western upper and middle slope are dominated by periplatform ooze (Fig. 12).

On the lower western slope, the deposits are limited to some pelagic and gravity deposits; MIS 5 in age. Sedimentation rates do not exceed 2 mm/kyr (Fig. 12). On the lower eastern slope, lobes consist of platform-derived coarse-grained sediments, which results in an increase in sedimentation rates in this area of up to <14 cm/kyr (Figs. 7 and 13).

Sediments at the GAC head are mainly composed of pelagic grains (Fig. 12). The fine fraction contains <5% of aragonite needles, and the sedimentation rates increase slightly northwards (Fig. 12). These sediments at the toe of the GAC mainly comprise hemipelagic deposits interbedded with rare fine-grained gravity-flow layers (Fig. 12).

Cores collected at the southern margin, however, record sequences enriched in platform-derived sediments, resulting in higher sedimentation rates during interglacials (Figs. 12 and 13). Gravity deposits enriched in slope-derived, highly-altered particles (Lantzsich et al., 2007) were recorded in the southern tributaries of the GAC (e.g., core CAR2KS09; Fig. 10). The carbonate-rich turbidite at the GAC outlet comprises pelagic and highly altered components (Fig. 9).

5. Discussion

5.1. GAC and northern LBB slope sedimentary dynamics

5.1.1. Sediment supply to the GAC

The structural control of the GAC incision has been previously discussed by Mullins et al. (1982), Mulder et al. (2018), and Recouvreur et al., 2020. Mullins et al. (1982) proposed that canyon walls were built during the Cretaceous by shallow-water organisms and walls erosion sustained the canyon incision. No platform-derived, coarse-grained gravity flows were recorded in Core CAR2KS14 during MIS 1 and 2 which correspond, respectively, to interglacial and glacial maxima, (Fig. 9). Therefore, a direct supply from the platform or the canyon walls does not agree with Mullins et al. (1982) hypothesis during the latest Pleistocene and Holocene.

Gravity currents flowing through GAC tributaries are rich in pelagic grains and lack platform-derived sediments since at least MIS 2–4; cores CAR2KS08 and CAR2KS09 collected in the GAC tributaries coming from the platform comprised sediments with slope-derived grains that were supplied through tributaries. Hence, the composition of the gravity flows in the tributaries during sea-level highstands seems to be independent of sediment production on the platform.

Mulder et al. (2018) and Recouvreur et al., 2020 proposed that sediment supply to sustain the canyon incision originates from the canyon tributaries and not from the canyon head. This sediment delivery process may explain the absence of platform-derived particles in the gravity flow deposit found at the GAC mouth (Fig. 9). The overall gravity-induced sediment export can be considered insignificant during the last glacials and interglacials throughout the GAC, except for sediment supply from the lateral tributaries (Fig. 9).

5.1.2. Differences between East and West of northern LBB

A set of morphological and structural hypotheses might explain the differences in facies distribution and sedimentation processes between the northeastern and northwestern slope of LBB. Tournadour et al. (2015) suggested that the presence of a rim along the eastern LBB slope (coral reef and shoals) is a significant controlling factor on the export of platform sediments with the rim limiting sediment export to specific reef channel outlets. A similar setting with shelf-edge barrier reefs limiting sediment export was discussed for the Ribbon Reef (Great Barrier Reef, NE Australia) by Puga-Bernabéu et al. (2011); this restriction in sediment export resulted in the development of steep exponential slopes. In contrast, south of Ribbon Reef within the Noggin region of the Great Barrier Reef (Puga-Bernabéu et al., 2013), slope-confined canyons with a sigmoidal slope shape developed at water depths between 200 and 400 m, as they are linked to an open outer-shelf without major barrier reefs. Tournadour et al. (2017) discussed canyon development processes with distinct retrogressive headward erosion similar to those observed for Ribbon Reef (Puga-Bernabéu et al., 2011). Austin Jr et al. (1988), Mulder et al. (2018) and Recouvreur et al., 2020 suggested that regional tectonic tilting coupled with differential subsidence westwards due to the presence of the GAC head could explain differences in subsidence resulting in differences in depositional processes occurring along the slope when moving from the east to the west (Figs. 11 and 12).

The western part of the LBB (“N-Western submerged LBB”, Fig. 1) corresponds to a fully submerged zone at <20 m water depth, extending over 10,500 km². This zone is dominated by packstone facies, with a fine-grained fraction that is exported to the slope in response to passing winter cold fronts. The eastern part of the LBB represents a submerged area that is ~9 times smaller than the western part due to the presence of the Abaco islands (1200 km²; “N-Eastern submerged LBB”, Fig. 1). In this area, the facies contains less fine-grained particles, is ooid-rich and comprises bioclast-rich shoals. Across the eastern LBB, the extent of packstones is limited to the areas between the grainstones and Abaco Island (170 km²; Fig. 1). The coarse-grained facies covers an area that is ~3.5 times larger (600 km²; Fig. 1) than the area occupied by the packstones. Thus, a close link can be observed between the platform facies and sedimentary process on the adjacent slopes with fine-grained export increasing when the shallow-water areas are dominated by fine-grained facies. Both the abundance of periplatform ooze on the north-western slope (Fig. 12) mobilized by density cascading and the higher sedimentation rates found on the western slope (Fig. 12) confirms this link between platforms facies and slope. A similar link between shallow-water facies distribution and sedimentary processes on the adjacent slope was established for Ribbon Reef and the Noggin Passage region (Great Barrier Reef, NE Australia) where the overall shape of the continental slope together with the presence (Ribbon Reef) or absence (Noggin Passage region) of shelf-edge barrier reefs resulted in differences in slope morphology. The Ribbon Reef sedimentary system lacking shelf-edge barrier reefs, produced a steep exponential slope as the restricted sediment export of the Noggin Passage system could be linked to a sigmoidal shaped slope. The presence of a large-scale MTD in the northwest possibly results from the high sediment export of fine-grained

sediments that cannot maintain high slope angles (Kenter, 1990). The study of Harwood and Towers (1988) discussing large- and small-scale slip on the LBB slope because of the high mud content of the slope deposits agrees with aforementioned slope adjustment processes linked to its mud content (Kenter, 1990).

Along the northern LBB upper and middle slope, gravity currents are rare and limited to the northeastern section (Fig. 12). The eastern slope angle averages 2.5° while the western slope average is 1.2° (Fig. 4).

5.1.3. The MIS 5 event

A coarse-grained layer with platform-derived grains present on the GAC southern margin (≈ 20 cm thick grainflow; Figs. 5 and 10) characterizes MIS 5 in cores CAR2KS01, CAR2KS02 and CAR2KS03 from the GAC head to the northern LBB slope. This layer suggests that a significant volume of platform-derived sediments were transported as a single event for over 50 km along the northern LBB slope during MIS 5. Similar large-scale gravity flow deposits were described by Crevello and Schlager (1980) for the Exuma Sound basin. These gravity-flow deposits, also dated as MIS 5, were enriched in coarse-grained platform-derived particles that showed no internal structures (Crevello and Schlager, 1980; Droxler, 1984). Two origins were proposed by Crevello and Schlager (1980) to explain these destabilizations: (i) the significant thickness of the deposit suggests a large-volume failure which could have been triggered by an earthquake or a tsunami, or (ii) a failure due to destabilization by local sediment overloading on the margin related to an increased productivity. Because of the large scale of the failures, an earthquake source appeared more likely according to Crevello and Schlager (1980). However, the Bahamas are considered a fair tectonic quiescent area (Masferro et al., 2002). Therefore, Spence and Tucker (1997) highlighted the importance of pore-water overpressure of confined aquifer horizons associated with karstification beneath the seafloor as the dominant factor of destabilization during sea-level falls. This process was also proposed in the modelling study of Busson et al. (2021) to explain the occurrence of platform margin collapses and associated MTD deposits, marking the western margin of GBB during sea-level falls. The pore-water overpressure scenario and associated platform margin sediment overloading were confirmed through the analysis of the debris-flow facies constituents by Reijmer et al. (2012, 2015a, 2015b), which explained the occurrence of debris-flow deposits at glacial to interglacial and interglacial to glacial transitions for Exuma Sound. Le Goff et al. (2021) unequivocally demonstrated the source and transport path of a shallow-water derived debris flow within Exuma Valley. The large-scale coarse-grained sediment transport processes are in line with the aforementioned small-scale resedimentation processes discussed for Exuma Sound and Exuma Valley.

5.2. Currents influence

5.2.1. Differences between glacial and interglacials

Bahamian slopes generally show higher sedimentation rates during interglacial periods resulting from high aragonite needles production and export from the flooded LBB platform (Schlager et al., 1994; Chabaud et al., 2015). This climate and linked sea-level related cyclic carbonate production and export is, however, not recorded in the GAC area, where interglacial and glacial periods cannot be distinguished based on sediment composition. The analysis of

platform-derived aragonite needles repartition shows that aragonite needles never exceed 5% of the fine-grained fraction on the lower slope and in deeper environments. Consequently, platform-derived supply cannot explain the slightly higher sedimentation rates during interglacial periods at the GAC area. These slightly higher sedimentation rates during interglacials probably result from a combination of processes: (i) better preservation of carbonates during interglacials (Chaisson et al., 2002; Franz and Tiedemann, 2002; Schwarz and Rendle-Bühring, 2005; Naik et al., 2017), and (ii) a decrease in the intensity of currents during interglacials favouring deposition (Chabaud et al., 2015). As platform-derived needles are produced when the platform is flooded, their occurrence during glacial periods is probably caused by stronger bottom currents that remobilize/ alter fine-grained sediments previously deposited on the slope (Fig. 13). As the GAC head receives no platform-derived sediment supply during both interglacials and glacials (Figs. 12 and 13), the highstand shedding sedimentation pattern does not apply northwards of the GAC incision and hence operates under more pelagic conditions. The equivalent limit of this area eastwards is unknown because sediment transfer across the LAC is not well known.

The seaward deposition of grains mobilized during sea-level high-stands is limited due to strong currents operating near the northern LBB. The Antilles Current seems to trap the platform-derived fine-grained fraction and transports it towards the LBB drift (Figs. 12 and 13). Water masses highly concentrated in aragonite needles apparently move from the platform to the slope, from the Holocene wedge to the west (Fig. 12). The extent of the periplatform ooze depositional area and the northwards decrease in sedimentation rates evidence that platform-derived sediments travel north-westwards. High sedimentation rates and sand content suggest preferential deposition of the platform-derived coarse-grained fraction in the MTC slide scar supplied by currents (Fig. 12). Platform input is limited to a maximum distance of 50 km northward of the platform edge (Figs. 12 and 13). This 50 km limit agrees with boundaries proposed for Pedro Bank (Caribbean; Andresen et al., 2003) and the Glorieuses archipelago (SW Indian Ocean; Jorry et al., 2020).

5.2.2. Origin of currents

Sedimentation rates gradually decrease northward because of the pirating effect of the Antilles Current. They increase slightly on the northern GAC head margin (Fig. 12). Thus, on the slope, the sedimentation rate decreases when the water depth increases. This correlation opposes the pattern found on the northern GAC margin, suggesting different operating sedimentary processes (Figs. 12 and 13). The northern GAC margin is draped by contourites; whose current influence affecting sediment deposition is still debated (Mulder et al., 2018; Recouvreur et al., 2020). The seafloor could be bathed either by the base of the Antilles Current or by the upper part of the DWBC (Fig. 1) considering that previous studies discussed that the water depth of the boundary between these two water masses varied through time (Table 4; Franz and Tiedemann, 2002; Yokokawa and Franz, 2002).

5.2.2.1. Detrital ratio evolution during Glacial Terminations.

Terminations I, II and III generally show higher contents in terrigenous elements than the sediments deposited during glacial periods in core CAR2KS13 (Fig. 6). Potassium classically marks the presence of illite in the clay assemblage (De Boedt et al., 1990), but despite similar variations during glacials, potassium does not systematically show an increase that is of the same order of terrigenous elements variation. Variations in illite content related to the NADW

circulation have been described for the Last Glacial Maximum (LGM; Fagel et al., 1997). The illite contents decreased from the LGM to MIS 1 due to variations in sedimentary sources at high latitudes; the source of illite in the NADW water body is mainly northern Greenland. Decrease in illite content in the NADW at the end of glacials is related to dilution by sediment from different sources, such as the Canadian or the Greenland margins (Fagel et al., 1997). Therefore, the illite variations seem to reflect the influence of the DWBC, the lower part of the NADW, on sedimentation patterns in the study area (Fig. 13).

The slow upwelling current, up to 10 cm/s, recorded by Mullins et al. (1982) for the GAC region could correspond to a part of the DWBC moving up the GAC from the abyssal plain and circulating on the Blake Plateau (Fig. 13). Those velocities are enough to transport microscopic elements, such as radiolarians skeletons (Popova, 1986). An upwelling current in the GAC would explain (i) the shift in deposition rates and sedimentary mechanisms from the northern to the southern GAC head (Fig. 12) and (ii) the presence of radiolarians at the confluence of GAC and tributaries. Consequently, most of seafloor sediments in our study area are primarily influenced by currents, and not by platform input (Fig. 13). Below 2000 m water depth, sedimentation is mainly controlled by the eddies of the Antilles Current (Johns et al., 1995), while the deepest part, from the GAC head to the abyssal plain, seems to be controlled by the DWBC.

5.2.2.2. Grain-size transition during the MIS 8.

MIS 8 is a unique marine isotope stage, being one of the warmer glacial isotope stages that is induced by a low variability in insolation (Lang and Wolff, 2011). Within the GAC head area, the grain-size spectrum changes from a dominant 2 μm -centred mode before MIS 8 to a dominant 63 μm -centred mode since MIS 8 (Figs. 9 and 10), however, no significant variations in the nature of the particles were observed. Studies on the Blake Outer Ridge (Fig. 1) highlighted grain-size variations during the glacial periods of MIS 8 and MIS 10 that were related to a vertical shift in the water depth level of the DWBC (Yokokawa and Franz, 2002; Table 4). At some intervals during MIS 8 and MIS 10, the DWBC body reached water depths shallower than ~ 2200 m, the depth of the mixing zone with the AABW (Franz and Tiedemann, 2002; Yokokawa and Franz, 2002; Table 4; Fig. 13). Therefore, the GAC head (~ 1700 m) was likely under the influence of the DWBC during these time intervals. The influence of AABW was not demonstrated on the Blake Outer Ridge since MIS 8, which suggests that the water depth at which the DWBC operated decreased. A process that probably started after MIS 8 and remained active until present day. Such a scenario agrees with the absence of a new shift in grain-size mode since this period on the northern LBB. Therefore, the preponderance of the silt fraction since MIS 8 can be explained by (i) either an increase in secondary producers after the decrease in the influence of AABW, or (ii) an increase in winnowing of the fine fraction (same features as terrigenous sediments; Faugères and Stow, 1993) following the general acceleration of the North Atlantic circulation during the last eight MIS.

5.2.2.3. Clay-rich layers.

Despite the modern abundance of almost pure carbonate sediments off the Bahamas since the Pleistocene, the seabed has experienced episodes with enriched clay deposition. For some periods and locations, this enrichment resulted in an increase in clay minerals concentration

within the carbonate ooze, as for example in the Straits of Florida during the Miocene (Swart et al., 2000; Karpoff et al., 2002).

Pelagic carbonate deposits with intercalated clay-rich layers occur within the GAC head and margins and are synchronous with pelagic carbonate deposits with clay-rich layers present on the Blake Outer Ridge further north (Fig. 1) that post-dated the Brunhes/Matuyama boundary (Keigwin et al., 1998a, 1998b). Clay-rich layers (Fig. 8), succeeding laminae made of altered silts to sands, appear in both areas (Keigwin et al., 1998; Fig. 1). The Blake Outer Ridge and the northern GAC head have similar sedimentation patterns since the Late Pleistocene, except for the presence of red lutites observed on the Blake Outer Ridge that are not present near the Bahamas. These levels are related to deglaciation deposits and can be a more local phenomenon (Keigwin et al., 1998a, 1998b). This suggests that the sedimentation patterns in the GAC area and the Blake Outer Ridge are similar. The presence of the DWBC on the Blake Outer Ridge is consistent with the DWBC influence on the GAC head.

Different processes may explain the deposition of the clay-rich deposits, such as the favoured transfer of clay particles into the marine environment, enhanced dissolution of carbonate particles, or a decrease in carbonate productivity. The silty sandy bases of MIS 7 and 9 clay-rich deposits characterized by non-determined bioclasts reflect a significant change in water bodies at the onset and during the Thermal Maxima Events (TMEs), and may be due to the sediment dissolution processes (Cronin et al., 2017).

The clay-rich layers present on the northern LBB were deposited during MIS 9 and 7. In Exuma Sound (Fig. 1), these periods are characterized by relatively low sedimentation rates compared to other interglacials (Reijmer et al., 1988). In the Arctic, the TMEs (Cronin et al., 2017), which are periods of significant cooling during interglacials, resulted in the development of ice sheets. The significant thickness of these ice sheets caused a deepening in the water depth of the downwelling warmer Atlantic water masses. As a result (i) the Atlantic waters warmed deeper bathymetries than during interglacial periods and (ii) the scenario prevented the communication between deep Arctic water masses and the surface waters, limiting oxygenation or supply of nutrients derived from surface productivity (Cronin et al., 2017). The most recent clay-rich level, dated MIS 7, would correspond to TME 3, as another clay-rich level, dated MIS 9, could correspond to TME 4. The occurrence of these cooling events during interglacials generated environmental conditions different from those occurring during glacials (sea level, soil formation and continental erosion) and could explain why the clays are not observed for glacial intervals. However, this does not explain why TM1 (MIS 5–4; Cronin et al., 2017) is not recorded in the study area. Hence, more information about the global ocean circulation during MIS 7 and 9 is needed to confirm if the occurrence of the clay-rich layers was generated by the TMEs.

5.3. Comparison with other Bahamian systems

The new core dataset for the northern LBB slope allows to highlight differences between northern LBB slope and other Bahamian slopes. Fig. 14 integrates the new findings with the interpretations obtained on the south-western GBB slope (Santaren channel; Wunsch et al., 2017, 2018), the eastern GBB slope (Florida Straits; Principaud et al., 2015, 2017, 2018; Le Goff et al., 2020), Exuma Sound and Exuma canyon (Crevello and Schlager, 1980; Cartwright, 1985; Le Goff et al., 2021) as well as earlier studies on the LBB slope (Chabaud et al., 2015; Tournadour et al., 2015, 2017; Fauquembergue et al., 2018).

The Antilles Current and DWBC have an impact on the seafloor morphology (carbonate mounds and drifts) and the distribution of Quaternary deposits on the northern LBB slope (pelagites, hemipelagites and contourites; Figs. 8, 9, 10 and 14; Eberli and Betzler, 2019; Mulder et al., 2019). The Bahamian platform-derived sediment export is generally fine-grained during sea-level highstands (Rendle-Bühning and Reijmer, 2005). The leeward western GBB facies are rich in mudstones and packstones, similar to those on the northwestern LBB. Coarse platform-derived sediments are preferentially deposited on slopes associated with leeward margins as hydrodynamic conditions support a general sedimentary transfer from the northeastern to the southwestern Bahamas, like the western GBB, explaining partially the highest sedimentation rates found there.

Along the western GBB slopes, platform export, which is particularly important in this leeward context, can result in the formation of sedimentary structures such as sediment waves or gullies formed by important export during sea-level highstands (Betzler et al., 2014; Wunsch et al., 2017, 2018; Figs. 2 and 14). Because the northwestern LBB slope is situated in a windward position, sediment export is limited and the development of similar sedimentary structures are lacking (Fig. 14). MTC's are the only deposits that can be found in both the windward and leeward setting, often related to sediment overloading that may occur with a relatively low frequency in any depositional setting (Principaud et al., 2015; Tournadour et al., 2015; Le Goff et al., 2020).

Exuma Sound and the Exuma Canyon are generally associated with the influx of platform-derived coarse-grained facies (Crevello and Schlager, 1980; Cartwright, 1985; Le Goff et al., 2021). This facies is also observed on the northeastern LBB slope, in the lobe that is formed downstream of this windward margin (Fig. 11). In both depositional systems the shallow parts of the platforms associated with the slopes are depleted in mud when compared to other Bahamian areas (Harris et al., 2015; Fig. 1). This confirms the results that were obtained on the northern LBB slope that (i) the dominant facies on the platforms is an important factor controlling slope facies and (ii) the wind direction is another important factor controlling the volume of grain export as shown for the western GBB slope (Rendle-Bühning and Reijmer, 2005).

In summary, it was observed that along the Bahamian slope, deposits enriched in platform-derived coarse-grained particles are not frequent. Mud-dominated sequences prevail and various processes generate sedimentary bedforms like sediment waves (western GBB), gullies and small channel-levee systems. Most of these sedimentary structures reflect high sediment export during highstands as the GBB is flooded and sediment production feeding the system is high.

The Eastern Cay Salt Bank slope is the only one that shows active channels during sea-level fall (Wunsch et al., 2017). Along this windward margin, presumably less active than a leeward margin during highstands as the bank is semi-drowned (Purkis et al., 2014), downwelling currents are particularly active during sea-level fall and remobilize older deposits, thus, their activity is controlled by currents.

Aragonite needles dominate the mud exported from platforms during the Holocene and occur with high percentages in the LBB northern uppermost slope wedge (>80% of total deposits; Figs. 3 and 4; Rankey and Doolittle, 2012; Mulder et al., 2017; Fauquembergue et al., 2018), and have lower percentages in the periplatform ooze present on the upper slope (~50% of total deposits; Figs. 3 and 4; Chabaud, 2016). A similar Holocene wedge rich in aragonite needles can be found along the northwestern GBB slope (Wilber et al., 1990; Roth and Reijmer, 2004, 2005). It is widespread and covers, with varying thickness, over >20 km on the western GBB as on the northern LBB it occupies <5 km (Rendle-Bühning and Reijmer, 2005; Principaud,

2015; Mulder et al., 2017). Holocene deposits are thicker along the western GBB, the wedge is continuous and can be up to 38 m thick (Roth and Reijmer, 2004, 2005; Principaud, 2015) than on the northwestern LBB which thickness vary spatially from 0 to 35 m, with a mean value of 15 (Mulder et al., 2017). On other slopes the Holocene deposits are thinner, for example on the Exuma Sound slope the Holocene sequence is <1 m thick (Droxler et al., 1988b; Reijmer et al., 1988). While the northwestern LBB and western GBB highlight a major influence of mud produced on the shallow-water platforms that are shaped by currents, the Exuma Basin is less influenced by mud export, but displays numerous coarse-grained gravity-flow deposits with bioclasts derived from the platform margins (Crevello and Schlager, 1980; Reijmer et al., 1988, 2012, 2015b; Droxler et al., 1988a, 1988b; Le Goff et al., 2020). The observed differences between the northeastern and northwestern LBB slope records confirmed that different sedimentation mechanisms operate on these slope sections. The differences between Exuma Sound slopes and northwestern LBB and GBB slopes could be due to the overall setting in which (i) less fine-grained sediments are available on platforms surrounding the Exuma Sound basin (Harris et al., 2015), and (ii) a steeper inclined slope promoting sediment bypass and gravity-induced sediment redeposition in the Exuma Sound basin (Rendle-Bühring and Reijmer, 2005). Hence, a distinct link exists between the facies distribution on the platform, the morphology at the platform margin, i.e., presence or absence of sand shoals, reefs or islands, the grain-size spectrum of the exported sediments and the slope morphology. The results agree with the outcome of studies by Puga-Bernabéu et al. (2011, 2013) for the Great Barrier Reef and Etienne et al. (2021) for Lansdowne Bank (SW Pacific Ocean).

6. Conclusions

Sediment core analysis enabled the interpretation of sedimentation patterns that occur along the northern LBB slopes and allowed for a comparison with other Bahamian slopes:

(1) Sediment availability on the platform is reflected in both the morphology of the northern LBB slope as well as the Quaternary sedimentation patterns. The scarcity of coarse-grained gravity flow deposits occurs north of LBB and within the giant GAC. Gravity deposits are restricted to the northeastern LBB slope, where no fine fraction sediments were available for export. The absence or presence of coarse platform grains on the northern LBB slope is conditioned by the distribution of shallow-water and platform margin facies. Other Bahamian slopes such as Exuma Sound exhibit a similar pattern related to the limited availability of fine grains on the bank resulting in the dominance of coarse-grained deposits on the deeper slopes. When carbonate mud export is high (e.g., leeward GBB) it can induce small and rare sedimentary structures like gullies as sediment export is efficient enough to produce such sedimentary features.

(2) Ocean current circulation is a dominant controlling factor on slope sedimentation on the northern LBB. The Antilles Current plays an active role in trapping carbonate mud produced on the platform, which is resuspended during passing cold fronts and hurricanes. The Antilles Current also redistributes the fine sediments along the upper and middle slopes and plays an important role in forming the LBB drift. Deposits around the GAC head and on the Blake Plateau are influenced by the DWBC. This could be a DWBC part coming from the Blake Outer Ridge bathing the Blake Plateau, or a current flowing up the GAC. The distribution of sediments produced on platform is limited to 50 km from the platform margin edge as known from various other carbonate systems, e.g. Pedro Bank (Caribbean), Glorieuses archipelago (Indian Ocean). Variations in current velocity are underlined by grain-size variation in the carbonate system

(highlighted by differences between MIS 8 vs MIS 10) similar to what is known from terrigenous systems.

(3) The continuity of clay-rich levels on the northern levee of the GAC as well as the Blake Outer Ridge suggests that two peculiar events occurred during the Thermal Maxima Events that affected sediment deposition during MIS 7 and MIS 9 on the Blake Plateau. These events are either due to the dissolution of carbonates or represent a sharp increase in clay input, or are formed by a decline in carbonate production.

(4) Sedimentation models of the different Bahamian slopes indicate that platform-derived sediment has an important impact on slope facies. Fine-grained dominated platform facies agree with fine-grained sediment export and smooth exponential slopes at which the sediments can be carried by current activity, whereas coarse-grained dominated platform facies is associated with coarse-grained sediment export and steep slopes.

Declaration of Competing Interest

The authors declare that they have no known competing financial interests or personal relationships that could have appeared to influence the work reported in this paper.

Data availability

Data obtained on cores and Very High Resolution profiles related to cores will not be placed in a data repository as private company (Total) funds most of them, and are not available without the authors approval, but can be on demand. Feel free to contact authors about this topic.

Acknowledgements

The authors thank the captain and crew of the R/V F.G. Walton Smith, R/V L'Atalante and R/V Le Suroît, as well as IFREMER (Brest, France) and Genavir (Plouzané, France) for their help with the acquisition of the data. TOTAL Research Laboratory (Pau, France) sponsored the data acquisition and subsequent laboratory analysis. This paper is part of the Ph.D. project of K. Fauquembergue that was funded by TOTAL (Pau, France). We also would like to thank Dr. Sebastian Lindhorst (Hamburg) for his work on the geoaoustic acquisition along the western GBB slope.

References

- Andresen, N., Reijmer, J.J.G., Droxler, A.W., 2003. Timing and distribution of calciturbidites around a deeply submerged carbonate platform in a seismically active setting (Pedro Bank, Northern Nicaragua Rise, Caribbean Sea). *Int. J. Earth Sci.* 92, 573–592. <https://doi.org/10.1007/s00531-003-0340-0>.
- Austin Jr., J.A., Schlager, W., Palmer, A.A., Comet, P.A., Droxler, A.W., 1988. Leg 101—An Overview. *Ocean Drilling Program, College Station*.

- Austin Jr., J.A., Schlager, W., Palmer, A.A., 1986. Proceedings of the Ocean Drilling Program, 101 Initial Reports, Proceedings of the Ocean Drilling Program. Ocean Drilling Program. <https://doi.org/10.2973/odp.proc.ir.101.1986>.
- Ball, 1967. Carbonate Sand Bodies of Florida and the Bahamas. *J. Sediment. Res.* 37 (2), 556–591. <https://doi.org/10.1306/74D7171C-2B21-11D7-8648000102C1865D>.
- Balsam, W.L., 1983. Carbonate Dissolution on the Muir Seamount (Western North Atlantic): Interglacial/Glacial changes. *J. Sediment. Res.* 53, 719–731. <https://doi.org/10.1306/212F82AB-2B24-11D7-8648000102C1865D>.
- Bates, R.L., Jackson, J.A., 1987. Glossary of Geology, 3rd ed. American Geological Institute. ed.
- Benson, W.E., Sheridan, R.E., 1975. Introduction and Principal Results (No. DSDP Vol 44).
- Bergman, K.L., 2005. Seismic Analysis of Paleocurrent Features in the Florida Straits : Insight into the Paleo-Florida Current, Upstream Tectonics, and the Atlantic- Caribbean Connection. University of Miami, RSMAS, Florida (PhD thesis.).
- Betzler, C., Lindhorst, S., Eberli, G.P., Ludmann, T., Mobius, J., Ludwig, J., Schutter, I., Wunsch, M., Reijmer, J.J.G., Hubscher, C., 2014. Periplatform drift: the combined result of contour current and off-bank transport along carbonate platforms. *Geology* 42, 871–874. <https://doi.org/10.1130/G35900.1>.
- Bilo, T.C., Johns, W.E., 2020. The deep western boundary current and adjacent interior circulation at 24°–30°N: mean structure and mesoscale variability. *J. Phys. Oceanogr.* 50, 2735–2758. <https://doi.org/10.1175/JPO-D-20-0094.1>.
- Bintanja, R., van de Wal, R.S.W., Oerlemans, J., 2005. Modelled atmospheric temperatures and global sea levels over the past million years. *Nature* 437, 125–128. <https://doi.org/10.1038/nature03975>.
- Bliefnick, D.M., Robertson, A.H.F., Sheridan, R.E., 1983. Deposition and provenance of Miocene intraclastic chinks, Blake-Bahama Basin, western North Atlantic. In: Initial Reports DSDP, Leg 76, Norfolk to Fort Lauderdale, pp. 727–748.
- Böhm, E., Lippold, J., Gutjahr, M., Frank, M., Blaser, P., Antz, B., Fohlmeister, J., Frank, N., Andersen, M.B., Deininger, M., 2015. Strong and deep Atlantic meridional overturning circulation during the last glacial cycle. *Nature* 517, 73–76. <https://doi.org/10.1038/nature14059>.
- Boss, S.K., Neumann, A.C., 1993. Impacts of Hurricane Andrew on carbonate platform environments, northern Great Bahama Bank. *Geology* 21, 897–900.
- Busson, J., Teles, V., Mulder, T., Joseph, P., Guy, N., Bouziat, A., Danquigny, C., Poli, E., Borgomano, J., 2021. Submarine landslides on a carbonate platform slope: forward numerical modelling of mechanical stratigraphy and scenarios of failure precondition. *Landslides* 18, 595–618. <https://doi.org/10.1007/s10346-020-01510-7>.
- Cartwright, R.A., 1985. Provenance and Sedimentology of Carbonate Turbidites from Two Deep Sea Fans, Bahamas. University of Miami, Coral Gables, Florida (PhD thesis.).
- Chabaud, L., 2016. Mod`ele stratigraphique and processus sédimentaires au Quaternaire sur deux pentes carbonatées des Bahamas (leeward and windward). Université de Bordeaux.
- Chabaud, L., Ducassou, E., Tournadour, E., Mulder, T., Reijmer, J.J.G., Conesa, G., Giraudeau, J., Hanquiez, V., Borgomano, J., Ross, L., 2015. Sedimentary processes determining the modern carbonate periplatform drift of Little Bahama Bank. *Mar. Geol.* 378, 213–229. <https://doi.org/10.1016/j.margeo.2015.11.006>.
- Chaisson, W.P., Poli, M.-S., Thunell, R.C., 2002. Gulf Stream and Western Boundary Undercurrent variations during MIS 10–12 at Site 1056, Blake-Bahama Outer Ridge. *Mar. Geol.* 189, 79–105. [https://doi.org/10.1016/S0025-3227\(02\)00324-9](https://doi.org/10.1016/S0025-3227(02)00324-9).
- Crevello, P.D., Schlager, W., 1980. Carbonate debris sheets and turbidites, Exuma Sound, Bahamas. *J. Sediment. Res.* 50, 1121–1148.
- Cronin, T.M., Dwyer, G.S., Caverly, E.K., Farmer, J., DeNinno, L.H., Rodriguez-Lazaro, J., Gemery, L., 2017. Enhanced Arctic Amplification Began at the Mid-Brunhes Event ~400,000 years ago. *Sci. Rep.* 7 <https://doi.org/10.1038/s41598-017-13821-2>.

- Croudace, I.W., Rindby, A., Rothwell, R.G., 2006. ITRAX: description and evaluation of a new multi-function X-ray core scanner. *Geol. Soc. Lond. Spec. Publ.* 267, 51–63.
- Cry, G.W., 1965. Tropical Cyclones of the North Atlantic Ocean: Tracks and Frequencies of Hurricanes and Tropical Storms, 1871–1963. U. S. Weather Bureau Technical Paper.
- De Boodt, M.F., Hayes, M.H.B., Herbillon, A., De Strooper, E.B.A., Tuck, J.J., 1990. Soil Colloids and their Associations in Aggregates, NATO ASI Series. Springer US, Boston, MA. <https://doi.org/10.1007/978-1-4899-2611-1>.
- Dravis, J.J., 1996. Rapidity of freshwater calcite cementation—implications for carbonate diagenesis and sequence stratigraphy. *Sediment. Geol.* 107, 1–10. [https://doi.org/10.1016/S0037-0738\(96\)00063-2](https://doi.org/10.1016/S0037-0738(96)00063-2).
- Droxler, A.W., 1984. Late Quaternary Glacial Cycles in the Bahamian Deep Basins and Un the Adjacent Atlantic Ocean. Coral Gables, Florida, Miami.
- Droxler, A.W., Schlager, W., 1985. Glacial versus interglacial sedimentation rates and turbidite frequency in the Bahamas. *Geology* 13, 799–802.
- Droxler, A.W., Schlager, W., Whallon, C.C., 1983. Quaternary aragonite cycles and oxygen-isotope record in Bahamian carbonate ooze. *Geology* 11, 235–239. Droxler, A.W., Morse, J.W., Kornicker, W.A., 1988a. Controls on carbonate mineral accumulation in Bahamian basins and adjacent Atlantic Ocean sediments. *J. Sediment. Res.* 58, 120–130.
- Droxler, A.W., Bruce, C.H., Sager, W.W., Watkins, D.H., 1988b. Pliocene-Pleistocene variations in aragonite content and planktonic oxygen-isotope record in Bahamian periplatform ooze, Hole 633A. In: Austin Jr., J.A., Schlager, W. (Eds.), *Proceedings of the Ocean Drilling Program, Scientific Results. Ocean Drilling Program, College Station, TX*, pp. 221–244.
- Dunham, R.J., 1962. Classification of Carbonate Rocks according to Depositional Textures. AAPG Spec. Vol. M 1: Classification of Carbonate Rocks-A Symposium, pp. 108–121.
- Eberli, G.P., Betzler, C., 2019. Characteristics of modern carbonate contourite drifts. *Sedimentology* 66, 1163–1191. <https://doi.org/10.1111/sed.12584>.
- Eberli, G.P., Ginsburg, R.N., 1987. Segmentation and coalescence of Cenozoic carbonate platforms, northwestern Great Bahama Bank. *Geology* 15, 75–79. [https://doi.org/10.1130/0091-7613\(1987\)15<75:SACOC>2.0.CO;2](https://doi.org/10.1130/0091-7613(1987)15<75:SACOC>2.0.CO;2).
- Eberli, G., Ginsburg, R.N., 1989. Cenozoic Progradation of Northwestern Great Bahama Bank, a Record of Lateral Platform Growth and Sea-Level Fluctuations. *Spec Publ Soc Econ Paleont Min*, p. 44.
- Embry, A.F., Klovan, J.E., 1970. A late Devonian reef tract on the northeastern Banks Island, N.W.T. *Bull. Can. Petrol. Geol.* 19, 730–781.
- Enos, P., 1974. Surface Sediment Facies of the Florida-Bahamas Plateau Map Series MC- 5, no. 4 edn. Geological Society of America.
- Etienne, S., Le Roy, P., Tournadour, E., Roest, W.R., Jorry, S., Collot, J., Patriat, M., Largeau, M.A., Roger, J., Clerc, C., Dechnick, B., Sanborn, K.L., Lepareur, F., Horowitz, J., Webster, J.M., Gaillot, A., 2021. Large-scale margin collapses along a partly drowned, isolated carbonate platform (Lansdowne Bank, SW Pacific Ocean). *Mar. Geol.* 436, 106477 <https://doi.org/10.1016/j.margeo.2021.106477>.
- Fagel, N., Hillaire-Marcel, C., Robert, C., 1997. Changes in the Western Boundary Undercurrent Outflow since the last Glacial Maximum, from smectite/illite ratios in deep Labrador Sea sediments. *Paleoceanography* 12, 79–96. <https://doi.org/10.1029/96PA02877>.
- Faugères, J.-C., Stow, D.A., 1993. Bottom-current-controlled sedimentation: a synthesis of the contourite problem. *Sediment. Geol.* 82, 287–297.
- Fauquembergue, K., 2018. Transferts sédimentaires sur une marge carbonatée moderne de la plate-forme `a la plaine abyssale : marge nord de Little Bahama Bank. Université de Bordeaux, Bahamas.
- Fauquembergue, K., Ducassou, E., Mulder, T., Hanquiez, V., Perello, M.-C., Poli, E., Borgomano, J., 2018. Genesis and growth of a carbonate Holocene wedge on the northern Little Bahama Bank. *Mar. Pet. Geol.* <https://doi.org/10.1016/j.marpetgeo.2018.05.013>.

- Ford, D., Williams, P., 2007. *Karst Hydrogeology and Geomorphology*, 578. John Wiley and Sons, Ltd.
- Franz, S.O., Tiedemann, R., 2002. Depositional changes along the Blake–Bahama Outer Ridge deep water transect during marine isotope stages 8 to 10 – links to the Deep Western Boundary Current. *Mar. Geol.* 189, 107–122. [https://doi.org/10.1016/S0025-3227\(02\)00325-0](https://doi.org/10.1016/S0025-3227(02)00325-0).
- Giraudeau, J., Christensen, B.A., Hermelin, O., Lange, C.B., Motoyama, I., 1998. Proceedings of the Ocean Drilling Program 175 Initial Reports (Initial Reports No. 175). Proceedings of the Ocean Drilling Program. <https://doi.org/10.2973/odp.proc.ir.175.1998>.
- Grammer, G.M., Ginsburg, R.N., Swart, P.K., McNeill, D.F., Jull, A.J.T.,
- Prezbindowski, D.R., 1993. Rapid growth rates of syndepositional marine aragonite cements in steep marginal slope deposits, Bahamas and Belize. *J. Sediment. Petrol.* 63, 983–989.
- Hardy, J., Henderson, K., 2003. Cold Front Variability in the Southern United States and the Influence of Atmospheric Teleconnection patterns. *Phys. Geogr.* 24, 120–137. <https://doi.org/10.2747/0272-3646.24.2.120>.
- Harris, P.M.M., Purkis, S.J., Ellis, J., Swart, P.K., Reijmer, J.J.G., 2015. Mapping bathymetry and depositional facies on Great Bahama Bank. *Sedimentology* 62, 566–589. <https://doi.org/10.1111/sed.12159>.
- Harwood, G.M., Towers, P.A., 1988. Seismic sedimentologic interpretation of a carbonate slope, north margin of Little Bahama Bank. In: Austin Jr., J.A., Schlager, W. (Eds.), Proceedings of the Ocean Drilling Program, Scientific Results. Ocean Drilling Program, College Station (TX), pp. 263–277.
- Heusser, L., Oppo, D., 2003. Millennial- and orbital-scale climate variability in southeastern United States and in the subtropical Atlantic during Marine Isotope Stage 5: evidence from pollen and isotopes in ODP Site 1059. *Earth Planet. Sci. Lett.* 214, 483–490. [https://doi.org/10.1016/S0012-821X\(03\)00389-3](https://doi.org/10.1016/S0012-821X(03)00389-3).
- Hickey, B.M., MacCready, P., Elliott, E., Kachel, N.B., 2000. Dense saline plumes in Exuma Sound, Bahamas. *J. Geophys. Res. Oceans* 105, 11471–11488. <https://doi.org/10.1029/2000JC900004>.
- Hine, A.C., Neumann, A.C., 1977. Shallow carbonate-bank-margin growth and structure, Little Bahama Bank, Bahamas. *AAPG Bull.* 61, 376–406.
- James, N.P., Choquette, P.W., 1983. Diagenesis 6. Limestones - the sea floor diagenetic environment. *Geosci. Can.* 10, 162–179.
- Johns, B., 2011. R/V Knorr Cruise KN-200-4 (Cruise report). Port Everglades, FL to Port Everglades, FL.
- Johns, W.E., Shay, T.J., Bane, J.M., Watts, D.R., 1995. Gulf Stream structure, transport, and recirculation near 68°W. *J. Geophys. Res.* 100, 817–838. <https://doi.org/10.1029/94JC02497>.
- Jorry, S.J., Jouet, G., Edinger, E.N., Toucanne, S., Counts, J.W., Miramontes, E., Courgeon, S., Vazquez Riveiros, N., Le Roy, P., Camoin, G.F., 2020. From platform top to adjacent deep sea: new source-to-sink insights into carbonate sediment production and transfer in the SW Indian ocean (Glorieuses archipelago). *Marine Geology* 423, 106–144.
- Kaczmarek, S.E., Hicks, M.K., Fullmer, S.M., Steffen, K.L., Bachtel, S.L., 2010. Mapping facies distributions on modern carbonate platforms through integration of multispectral Landsat data, statistics-based unsupervised classifications, and surface sediment data. *AAPG Bull.* 94, 1581–1606. <https://doi.org/10.1306/04061009175>.
- Karpoff, A.M., Destrigneville, C., Bartier, D., Déjardin, P., 2002. Phyllosilicates and zeolite assemblages in the carbonate periplatform of the Great Bahama Bank: origin and relation to diagenetic processes (ODP Leg 166, Sites 1006 and 1007). *Mar. Geol.* 185, 55–74. [https://doi.org/10.1016/S0025-3227\(01\)00290-0](https://doi.org/10.1016/S0025-3227(01)00290-0).
- Keigwin, L.D., Rio, D., Acton, G.D., 1998a. Proceedings of the Ocean Drilling Program 172 Initial Reports : Bermuda Rise and Sohm Abyssal Plain, Sites 1063 and 1064. <https://doi.org/10.2973/odp.proc.ir.172.1998>.
- Keigwin, L.D., Rio, D., Acton, G.D., 1998b. Proceedings of the Ocean Drilling Program 172 Initial Reports : Summary, pp. 311–321. <https://doi.org/10.2973/odp.proc.ir.172.1998>.

- Kenter, J.A.M., 1990. Carbonate platform flanks: slope angle and sediment fabric. *Sedimentology* 37, 777–794. <https://doi.org/10.1111/j.1365-3091.1990.tb01825.x>. Kievman, C.M., 1998. Match between late Pleistocene Great Bahama Bank and deep-sea oxygen isotope records of sea level. *Geology* 26, 635–638. [https://doi.org/10.1130/0091-7613\(1998\)026<0635:MBLPGB>2.3.CO;2](https://doi.org/10.1130/0091-7613(1998)026<0635:MBLPGB>2.3.CO;2).
- Labourdette, R., Lascu, I., Mylroie, J., Roth, M., 2007. Process-like modeling of flank margin caves: from genesis to burial evolution. *J. Sediment. Res.* 77, 965–979. Lang, N., Wolff, E.W., 2011. Interglacial and glacial variability from the last 800 ka in marine, ice and terrestrial archives. *Clim. Past* 7, 361–380. <https://doi.org/10.5194/cp-7-361-2011>.
- Lantzsch, H., Roth, S., Reijmer, J.J.G., Kinkel, H., 2007. Sea-level related resedimentation processes on the northern slope of Little Bahama Bank (Middle Pleistocene to Holocene). *Sedimentology* 54, 1307–1322. <https://doi.org/10.1111/j.1365-3091.2007.00882.x>.
- Le Goff, J., Slooman, A., Mulder, T., Cavailles, T., Ducassou, E., Hanquiez, V., Jaballah, J., Reijmer, J.J.G., 2020. On the architecture of intra-formational Mass- Transport deposits: Insights from the carbonate slopes of Great Bahama Bank and the Apulian Carbonate Platform. *Mar. Geol.* 427, 106205 <https://doi.org/10.1016/j.margeo.2020.106205>.
- Le Goff, J., Recouvreur, A., Reijmer, J.J.G., Mulder, T., Ducassou, E., Perello, M., Hanquiez, V., Gillet, H., Cavailles, T., Fabregas, N., 2021. Linking carbonate sediment transfer to seafloor morphology: insights from Exuma Valley, the Bahamas. *Sedimentology* 68, 609–638. <https://doi.org/10.1111/sed.12794>.
- Lisiecki, L.E., Raymo, M.E., 2005. Correction to “A Pliocene-Pleistocene stack of 57 globally distributed benthic $\delta^{18}O$ records”. *Paleoceanography* 20, 1–17. <https://doi.org/10.1029/2005PA001164>.
- Major, R.P., Bebout, D.G., Harris, P.M., 1996. Recent evolution of a Bahamian ooid shoal: Effects of Hurricane Andrew. *Geol. Soc. Am. Bull.* 108, 168–180.
- Masaferro, J.L., Poblet, J., Bulnes, M., Eberli, G.P., Dixon, T.H., McClay, K.E.N., 1999. Palaeogene-Neogene/present day(?) growth folding in the Bahamian foreland of the Cuban fold and thrust belt. *J. Geol. Soc.* 156, 617–631. <https://doi.org/10.1144/gsjgs.156.3.0617>.
- Masaferro, J.L., Bulnes, M., Poblet, J., Eberli, G.P., 2002. Episodic folding inferred from syntectonic carbonate sedimentation: the Santaren anticline, Bahamas foreland. *Sediment. Geol.* 146, 11–24. [https://doi.org/10.1016/S0037-0738\(01\)00163-4](https://doi.org/10.1016/S0037-0738(01)00163-4).
- Meinen, C.S., Garzoli, S.L., Johns, W.E., Baringer, M.O., 2004. Transport variability of the deep western boundary current and the antilles current off Abaco Island, Bahamas. *Deep Sea Res. Part Oceanogr. Res. Pap.* 51, 1397–1415. <https://doi.org/10.1016/j.dsr.2004.07.007>.
- Meinen, C.S., Johns, W.E., Moat, B.I., Smith, R.H., Johns, E.M., Rayner, D., Frajka-Williams, E., Garcia, R.F., Garzoli, S.L., 2019. Structure and Variability of the Antilles current at 26.5°N. *J. Geophys. Res. Oceans* 124, 3700–3723. <https://doi.org/10.1029/2018JC014836>.
- Michel, J., Borgomano, J., Reijmer, J.J.G., 2018. Heterozoan carbonates: when, where and why? A synthesis on parameters controlling carbonate production and occurrences. *Earth-Sci. Rev.* 182, 50–67. <https://doi.org/10.1016/j.earscirev.2018.05.003>.
- Migeon, S., Weber, O., Faugeres, J.-C., Saint-Paul, J., 1998. SCOPIX: a new X-ray imaging system for core analysis. *Geo-Mar. Lett.* 18, 251–255. <https://doi.org/10.1007/s003670050076>.
- Mulder, T., Ducassou, E., Gillet, H., Hanquiez, V., Tournadour, E., Combes, J., Eberli, G. P., Kindler, P., Gonthier, E., Conesa, G., Robin, C., Sianipar, R., Reijmer, J.J.G., François, A., 2012. Canyon morphology on a modern carbonate slope of the Bahamas: evidence of regional tectonic tilting. *Geology* 40, 771–774. <https://doi.org/10.1130/G33327.1>.
- Mulder, T., Joumes, M., Hanquiez, V., Gillet, H., Reijmer, J.J.G., Tournadour, E., Chabaud, L., Principaud, M., Schnyder, J.S.D., Borgomano, J., Fauquembergue, K., Ducassou, E., Busson, J., 2017. Carbonate slope morphology revealing sediment transfer from bank-to-slope (Little Bahama Bank, Bahamas). *Mar. Pet. Geol.* 83, 26–34. <https://doi.org/10.1016/j.marpetgeo.2017.03.002>.
- Mulder, T., Gillet, H., Hanquiez, V., Ducassou, E., Fauquembergue, K., Principaud, M., Conesa, G., Le Goff, J., Ragusa, J., Bashah, S., Bujan, S., Reijmer, J.J.G.,

- Cavailhes, T., Droxler, A.W., Blank, D.G., Guiastrennec, L., Fabregas, N., Recouvreux, A., Seibert, C., 2018. Carbonate slope morphology revealing a giant submarine canyon (Little Bahama Bank, Bahamas). *Geology* 46, 31–34. <https://doi.org/10.1130/G39527.1>.
- Mulder, T., Ducassou, E., Hanquiez, V., Principaud, M., Fauquembergue, K., Tournadour, E., Chabaud, L., Reijmer, J., Recouvreux, A., Gillet, H., Borgomano, J., Schmitt, A., Moal, P., 2019. Contour current imprints and contourite drifts in the Bahamian archipelago. *Sedimentology* 66, 1192–1221. <https://doi.org/10.1111/sed.12587>.
- Mullins, H.T., Cook, H.E., 1986. Carbonate apron models: Alternatives to the submarine fan model for paleoenvironmental analysis and hydrocarbon exploration. *Sediment. Geol.* 48, 37–79. [https://doi.org/10.1016/0037-0738\(86\)90080-1](https://doi.org/10.1016/0037-0738(86)90080-1).
- Mullins, H.T., Neumann, A.C., 1979. Deep carbonate bank margin structure and sedimentation in the Northern Bahamas. In: Doyle, L.J., Pilkey, O.H. (Eds.), *Geology of Continental Slopes*. SEPM (Society for Sedimentary Geology), Tulsa, Oklahoma, U. S.A., pp. 165–192.
- Mullins, H.T., Neumann, A.C., Wilber, R.J., Hine, A.C., Chinburg, S.J., 1980. Carbonate sediment drifts in Northern Straits of Florida. *Am. Assoc. Pet. Geol. Bull.* 64, 1701–1717.
- Mullins, H.T., Keller, G.H., Kofoed, J.W., Lambert, D.N., Stubblefield, W.L., Warme, J.E., 1982. +. *Geology of Great Abaco Submarine Canyon (Blake Plateau): Observations from the research submersible “Alvin.”*. *Mar. Geol.* 48, 239–257. [https://doi.org/10.1016/0025-3227\(82\)90099-8](https://doi.org/10.1016/0025-3227(82)90099-8).
- Myroie, J.E., Carew, J.L., 1995. Karst development on carbonate islands 1 (2). In: Budd, D.A., Saller, A.H., Harris, P.A. (Eds.), *Unconformities in Carbonate Strata – Their Recognition and the Significance of Associated Porosity*, AAPG Memoir 63. Tulsa, Oklahoma, U.S.A., pp. 55–76.
- Naik, D.K., Saraswat, R., Lea, D.W., Kurtarkar, S.R., Mackensen, A., 2017. Last glacial- interglacial productivity and associated changes in the eastern Arabian Sea. *Palaeogeogr. Palaeoclimatol. Palaeoecol.*, Development, evaluation and application of marine paleoclimatic/paleoceanographic proxies: An update 483, 147–156. <https://doi.org/10.1016/j.palaeo.2016.07.014>.
- Neuendorf, K.K.E., Mehl, J.P., Jackson, J.A. (Eds.), 2011. *Glossary of Geology*. American Geosciences Inst, Alexandria, Virginia.
- Oppo, D.W., Keigwin, L.D., McManus, J.F., 2001. Persistent suborbital climate variability in marine isotope stage 5 and termination II. *Paleoceanography* 16, 280–292. <https://doi.org/10.1029/2000PA000527>.
- Park, L.E., 2012. Comparing two long-term hurricane frequency and intensity records from San Salvador Island, Bahamas. *J. Coast. Res.* 28 (4), 891–902. <https://doi.org/10.2112/JCOASTRES-D-11-00065.1>.
- Park, L.E., Siewers, F.D., Metzger, T., Sipahioglu, S., 2009. After the hurricane hits: Recovery and response to large storm events in a saline lake, San Salvador Island, Bahamas. *Quat. Int., Hurricanes Typhoons: Field Records Forecast* 195, 98–105. <https://doi.org/10.1016/j.quaint.2008.06.010>.
- Paul, A., Reijmer, J.J.G., Fürstenau, J., Kinkel, H., Betzler, C., 2012. Relationship between late Pleistocene Sea-level variations, carbonate platform morphology and aragonite production (Maldives, Indian Ocean): Sea-level and aragonite on the Maldives. *Sedimentology* 59, 1640–1658. <https://doi.org/10.1111/j.1365-3091.2011.01319.x>.
- Perkins, R.D., Enos, P., 1968. Hurricane Betsy in the Florida-Bahama Area: Geologic Effects and Comparison with Hurricane Donna. *J. Geol.* 76, 710–717. <https://doi.org/10.1086/627394>.
- Playton, T., Janson, X., Kerans, C., 2010. Carbonate slopes. In: *Facies Models 4*. Noel James, Roger Dalrymple, pp. 449–476.
- Popova, I.M., 1986. Transportation of radiolarian shells by currents (calculations based on the example of the Kuroshio). In: *Mar. Micropaleontol., EURORAD IV Fourth International Meeting of Radiolarists*, 11, pp. 197–201. [https://doi.org/10.1016/0377-8398\(86\)90014-9](https://doi.org/10.1016/0377-8398(86)90014-9).
- Principaud, M., 2015. Morphologie, architecture et dynamique sédimentaire d’une pente carbonatée moderne: le Great Bahama Bank (Bahamas). Université de Bordeaux.
- Principaud, M., 2016. Synthèse sédimentaire sur les pentes carbonatées bahamiennes : pente ouest du Great Bahama Bank and pente nord du Little Bahama Bank. Université de Bordeaux.

- Principaud, M., Mulder, T., Gillet, H., Borgomano, J., 2015. Large-scale carbonate submarine mass-wasting along the northwestern slope of the Great Bahama Bank (Bahamas): Morphology, architecture, and mechanisms. *Sediment. Geol.* 317, 27–42. <https://doi.org/10.1016/j.sedgeo.2014.10.008>.
- Principaud, M., Ponte, J.-P., Mulder, T., Gillet, H., Robin, C., Borgomano, J., 2017. Slope- to-basin stratigraphic evolution of the northwestern Great Bahama Bank (Bahamas) during the Neogene to Quaternary: interactions between downslope and bottom currents deposits. *Basin Res.* 29, 699–724. <https://doi.org/10.1111/bre.12195>.
- Principaud, M., Mulder, T., Hanquiez, V., Ducassou, E., Eberli, G.P., Chabaud, L., Borgomano, J., 2018. Recent morphology and sedimentary processes along the western slope of Great Bahama Bank (Bahamas). *Sedimentology* 65, 2088–2116. <https://doi.org/10.1111/sed.12458>.
- Puga-Bernabéu, A., Webster, J.M., Beaman, R.J., Guilbaud, V., 2011. Morphology and controls on the evolution of a mixed carbonate–siliciclastic submarine canyon system, Great Barrier Reef margin, North-Eastern Australia. *Mar. Geol.* 289, 100–116.
- Puga-Bernabéu, A., Webster, J.M., Beaman, R.J., Guilbaud, V., 2013. Variation in canyon morphology on the Great Barrier Reef margin, North-Eastern Australia: the influence of slope and barrier reefs. *Geomorphology* 191, 35–50.
- Puga-Bernabéu, A., Webster, J.M., Beaman, R.J., Reimer, P.J., Renema, W., 2014. Filling the gap: a 60 ky record of mixed carbonate-siliciclastic turbidite deposition from the Great Barrier Reef. *Mar. Pet. Geol.* 50, 40–50. <https://doi.org/10.1016/j.marpetgeo.2013.11.009>.
- Pujos, A., 1988. Spatio-temporal distribution of some Quaternary coccoliths. *Oceanol. Acta* 11, 65–77.
- Purkis, S., Kerr, J., Dempsey, A., Calhoun, A., Metsamaa, L., Riegl, B., Kourafalou, V., Bruckner, A., Renaud, P., 2014. Large-scale carbonate platform development of Cay Sal Bank, Bahamas, and implications for associated reef geomorphology. *Geomorphology* 222, 25–38.
- Rankey, E.C., Doolittle, D.F., 2012. Geomorphology of carbonate platform-marginal uppermost slopes: Insights from a Holocene analogue, Little Bahama Bank, Bahamas: Uppermost carbonate platform slope, Bahamas. *Sedimentology* 59, 2146–2171. <https://doi.org/10.1111/j.1365-3091.2012.01338.x>.
- Rankey, E.C., Enos, P., Steffen, K., Druke, D., 2004. Lack of impact of hurricane Michelle on tidal flats, Andros Island, Bahamas: integrated remote sensing and field observations. *J. Sediment. Res.* 74, 654–661.
- Ravenne, C., 2002. Stratigraphy and Oil: a Review - part 2: Characterization of Reservoirs and Sequence Stratigraphy: Quantification and Modeling. *Oil Gas Sci. Technol.* 57, 311–340. <https://doi.org/10.2516/ogst:2002021>.
- Ravenne, C., Le Quellec, P., Valery, P., 1985. Dépo[^]ts carbonatés profonds des Bahamas. In: Presented at the G[^]Odymanique Des Caraïbes. Technip, Symposium Paris.
- Recouvreur, A., Fabregas, N., Mulder, T., Hanquiez, V., Fauquembergue, K., Tournadour, E., Gillet, H., Borgomano, J., Poli, E., Kucharski, J.-B., Wilk, S., 2020. Geomorphology of a modern carbonate slope system and associated sedimentary processes: example of the giant Great Abaco Canyon, Bahamas. *Sedimentology* 68, 266–293.
- Reeder, S.L., Rankey, E.C., 2008. Interactions between tidal flows and Ooid Shoals, Northern Bahamas. *J. Sediment. Res.* 78, 175–186. <https://doi.org/10.2110/jsr.2008.020>.
- Reeder, S.L., Rankey, E.C., 2009. Controls on morphology and sedimentology of carbonate tidal deltas, Abacos, Bahamas. *Mar. Geol.* 267, 141–155. <https://doi.org/10.1016/j.margeo.2009.09.010>.
- Reijmer, J.J.G., 2021. Marine carbonate factories: Review and update. *Sedimentology* 68, 1729–1796. <https://doi.org/10.1111/sed.12878>.
- Reijmer, J.J.G., Schlager, W., Droxler, A.W., 1988. Site 632: Pliocene-Pleistocene sedimentation cycles in a Bahamian basin. In: Austin Jr., J.A., Schlager, W. (Eds.), *Proceedings of the Ocean Drilling Program, Scientific Results Leg 101*. Ocean Drilling Program, College Station (TX), pp. 213–220.
- Reijmer, J.J.G., Swart, P.K., Bauch, T., Otto, R., Reuning, L., Roth, S., Zechel, S., 2009. A Re-Evaluation of Facies on Great Bahama Bank I: New Facies Maps of Western Great Bahama Bank. In: Swart, P.K.,

- Eberli, G.P., McKenzie, J.A., Jarvis, I., Stevens, T. (Eds.), *Perspectives in Carbonate Geology*. John Wiley & Sons, Ltd, Chichester, West Sussex, UK, pp. 29–46. <https://doi.org/10.1002/9781444312065.ch3>.
- Reijmer, J.J.G., Palmieri, P., Groen, R., 2012. Compositional variations in calciturbidites and calcidebrites in response to sea-level fluctuations (Exuma Sound, Bahamas). *Facies* 58, 493–507. <https://doi.org/10.1007/s10347-011-0291-z>.
- Reijmer, Mulder, T., Borgomano, J., 2015a. Carbonate slopes and gravity deposits. *Sediment. Geol.* 315, 83–90. <https://doi.org/10.1016/j.sedgeo.2014.10.011>.
- Reijmer, Palmieri, P., Groen, R., Floquet, M., 2015b. Calciturbidites and calcidebrites: sea-level variations or tectonic processes? *Sediment. Geol.* 317, 53–70. <https://doi.org/10.1016/j.sedgeo.2014.10.013>.
- Rendle-Bühning, R.H., Reijmer, J.J.G., 2005. Controls on grain-size patterns in periplatform carbonates: marginal setting versus glacio-eustacy. *Sediment. Geol.* 175, 99–113. <https://doi.org/10.1016/j.sedgeo.2004.12.025>.
- Reolid, J., Betzler, C., Eberli, G.P., Grammer, G.M., 2017. The importance of microbial binding in neogene–quaternary steep slopes. *J. Sediment. Res.* 87, 567–577. <https://doi.org/10.2110/jsr.2017.28>.
- Roth, S., Reijmer, J.J.G., 2004. Holocene Atlantic climate variations deduced from carbonate periplatform sediments (leeward margin, Great Bahama Bank). *Paleoceanography* 19, PA1003. <https://doi.org/10.1029/2003PA000885>.
- Roth, S., Reijmer, J.J.G., 2005. Holocene millennial to centennial carbonate cyclicity recorded in slope sediments of the Great Bahama Bank and its climatic implications: Holocene carbonate cyclicity. *Sedimentology* 52, 161–181. <https://doi.org/10.1111/j.1365-3091.2004.00684.x>.
- Schlager, W., 2003. Benthic carbonate factories of the Phanerozoic. *Int. J. Earth Sci.* 92, 445–464. <https://doi.org/10.1007/s00531-003-0327-x>.
- Schlager, W., Ginsburg, R.N., 1981. Bahama carbonate platforms—the deep and the past. *Mar. Geol.* 44, 1–24.
- Schlager, W., Reijmer, J.J.G., Droxler, A.W., 1994. Highstand shedding of carbonate platforms. *J. Sediment. Res.* 64B, 270281 <https://doi.org/10.1306/D4267FAA-2B26-11D7-8648000102C1865D>.
- Schwarz, J., Rendle-Bühning, R., 2005. Controls on modern carbonate preservation in the southern Florida Straits. *Sediment. Geol.* 175, 153–167. <https://doi.org/10.1016/j.sedgeo.2004.12.024>.
- Shinn, E.A., Steinen, R.P., Dill, R.F., Major, R., 1993. Lime-mud layers in high-energy tidal channels: a record of hurricane deposition. *Geology* 21, 603–606.
- Spence, G.H., Tucker, M.E., 1997. Genesis of limestone megabreccias and their significance in carbonate sequence stratigraphic models: a review. *Sediment. Geol.* 112, 163–193. [https://doi.org/10.1016/S0037-0738\(97\)00036-5](https://doi.org/10.1016/S0037-0738(97)00036-5).
- Proceedings of the Ocean Drilling Program, 166 Scientific Results. In: Swart, P.K., Eberli, G.P., Malone, M.J., Sarg, J.F. (Eds.), 2000. *Proceedings of the Ocean Drilling Program*. Ocean Drilling Program. <https://doi.org/10.2973/odp.proc.sr.166.2000>.
- Toomey, M.R., Curry, W.B., Donnelly, J.P., Hengstum, P.J., 2013. Reconstructing 7000 years of North Atlantic hurricane variability using deep-sea sediment cores from the western Great Bahama Bank. *Paleoceanography* 28, 31–41.
- Tournadour, E., 2015. Architecture and dynamique sédimentaire d’une pente carbonatée moderne: exemple de la pente Nord de Little Bahama Bank, Bahamas. Bordeaux.
- Tournadour, E., Mulder, T., Borgomano, J., Hanquiez, V., Ducassou, E., Gillet, H., 2015. Origin and architecture of a Mass Transport complex on the northwest slope of Little Bahama Bank (Bahamas): Relations between off-bank transport, bottom current sedimentation and submarine landslides. *Sediment. Geol.* 317, 9–26. <https://doi.org/10.1016/j.sedgeo.2014.10.003>.
- Tournadour, E., Mulder, T., Borgomano, J., Gillet, H., Chabaud, L., Ducassou, E., Hanquiez, V., Etienne, S., 2017. Submarine canyon morphologies and evolution in modern carbonate settings: the northern slope of Little Bahama Bank, Bahamas. *Mar. Geol.* 391, 76–97. <https://doi.org/10.1016/j.margeo.2017.07.014>.

- Weaver, P.P.E., 1983. An integrated stratigraphy of the Upper Quaternary of the King's Trough flank area NE Atlantic. *Oceanol. Acta* 6, 451–4566. <https://archimer.ifremer.fr/doc/00120/23131/20978.pdf>.
- Wilber, R.J., Milliman, J.D., Halley, R.B., 1990. Accumulation of bank-top sediment on the western slope of Great Bahama Bank: rapid progradation of a carbonate megabank. *Geology* 18, 970–974.
- Wilson, P.A., Roberts, H.H., 1992. Carbonate-periplatform sedimentation by density flows: a mechanism for rapid off-bank and vertical transport of shallow-water fines. *Geology* 20, 713–716.
- Wilson, P.A., Roberts, H.H., 1995. Density cascading: off-shelf sediment transport, evidence and implications, Bahama Banks. *J. Sediment. Res.* 65A, 45–56. <https://doi.org/10.1306/D426801D-2B26-11D7-8648000102C1865D>.
- Wunsch, M., Betzler, C., Lindhorst, S., Lüdmann, T., Eberli, G.P., 2017. Sedimentary dynamics along carbonate slopes (Bahamas archipelago). *Sedimentology* 64, 631–657. <https://doi.org/10.1111/sed.12317>.
- Wunsch, M., Betzler, C., Eberli, G.P., Lindhorst, S., Lüdmann, T., Reijmer, J.J.G., 2018. Sedimentary dynamics and high-frequency sequence stratigraphy of the southwestern slope of Great Bahama Bank. *Sediment. Geol.* 363, 96–117. <https://doi.org/10.1016/j.sedgeo.2017.10.013>.
- Yokokawa, M., Franz, S.-O., 2002. Changes in grain size and magnetic fabric at Blake–Bahama Outer Ridge during the late Pleistocene (marine isotope stages 8–10). *Mar. Geol.* 189, 123–144. [https://doi.org/10.1016/S0025-3227\(02\)00326-2](https://doi.org/10.1016/S0025-3227(02)00326-2).

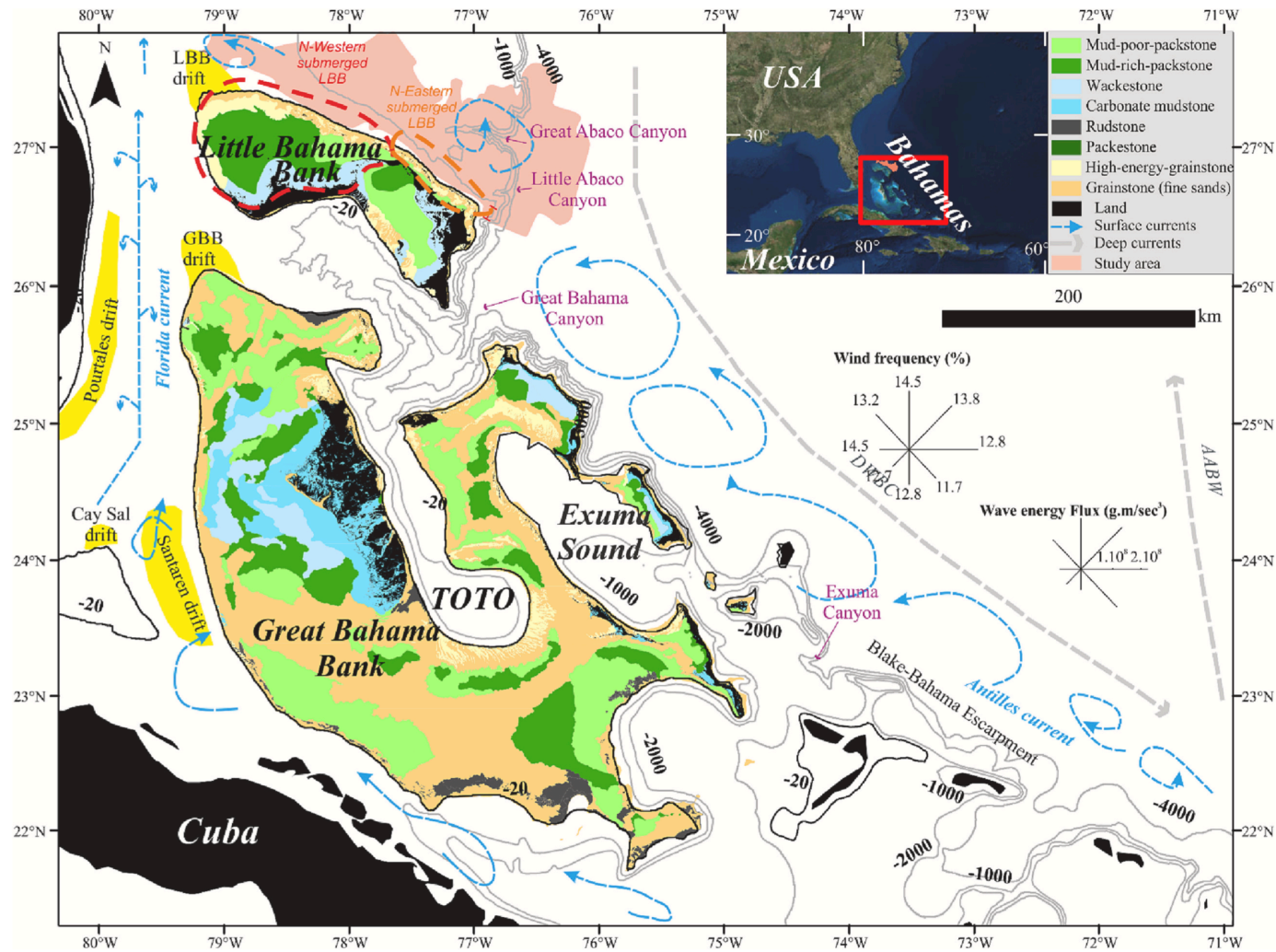


Fig. 1. Location map of the Bahamas (inset) and the study area (main map). Sediment distribution map of the present-day Bahamian platforms (colours see legend). After: Ball, 1967; Enos, 1974; Reijmer et al., 2009; Kaczmarek et al., 2010; Harris et al., 2015; Tournadour, 2015; synthesized by Principaud, 2016). Canyons names and current directions (blue arrows), and location and name of main drifts (yellow) are also indicated. TOTO: Tongue of the Ocean. AABW: Antarctic Bottom Water. DBWC: Deep Western Boundary Current. Water depth in metres.

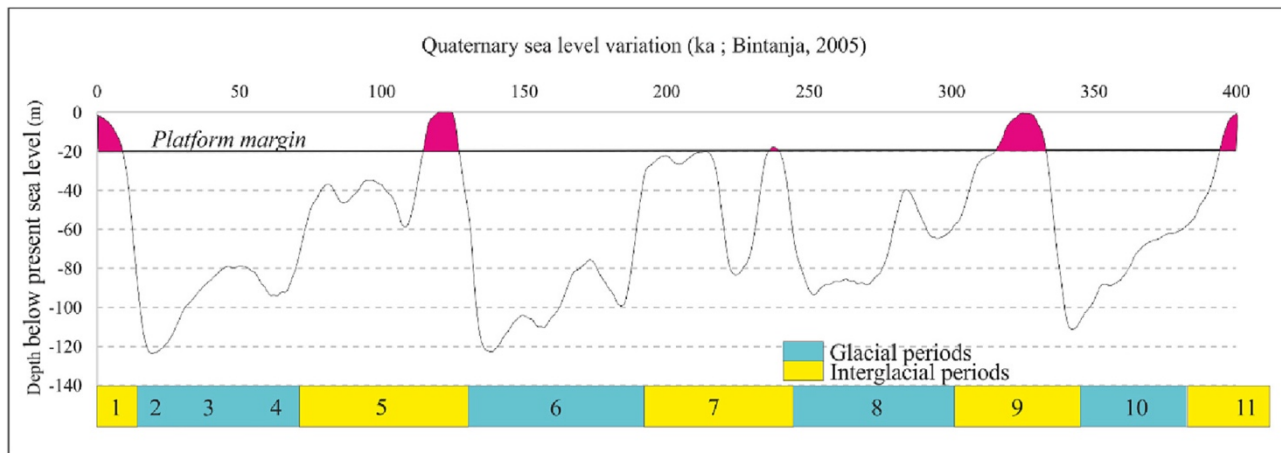


Fig. 2. Sea-level variation (Bintanja et al., 2005) and time intervals when Bahamian platforms were flooded (pink time intervals) for the last 400 kyr.

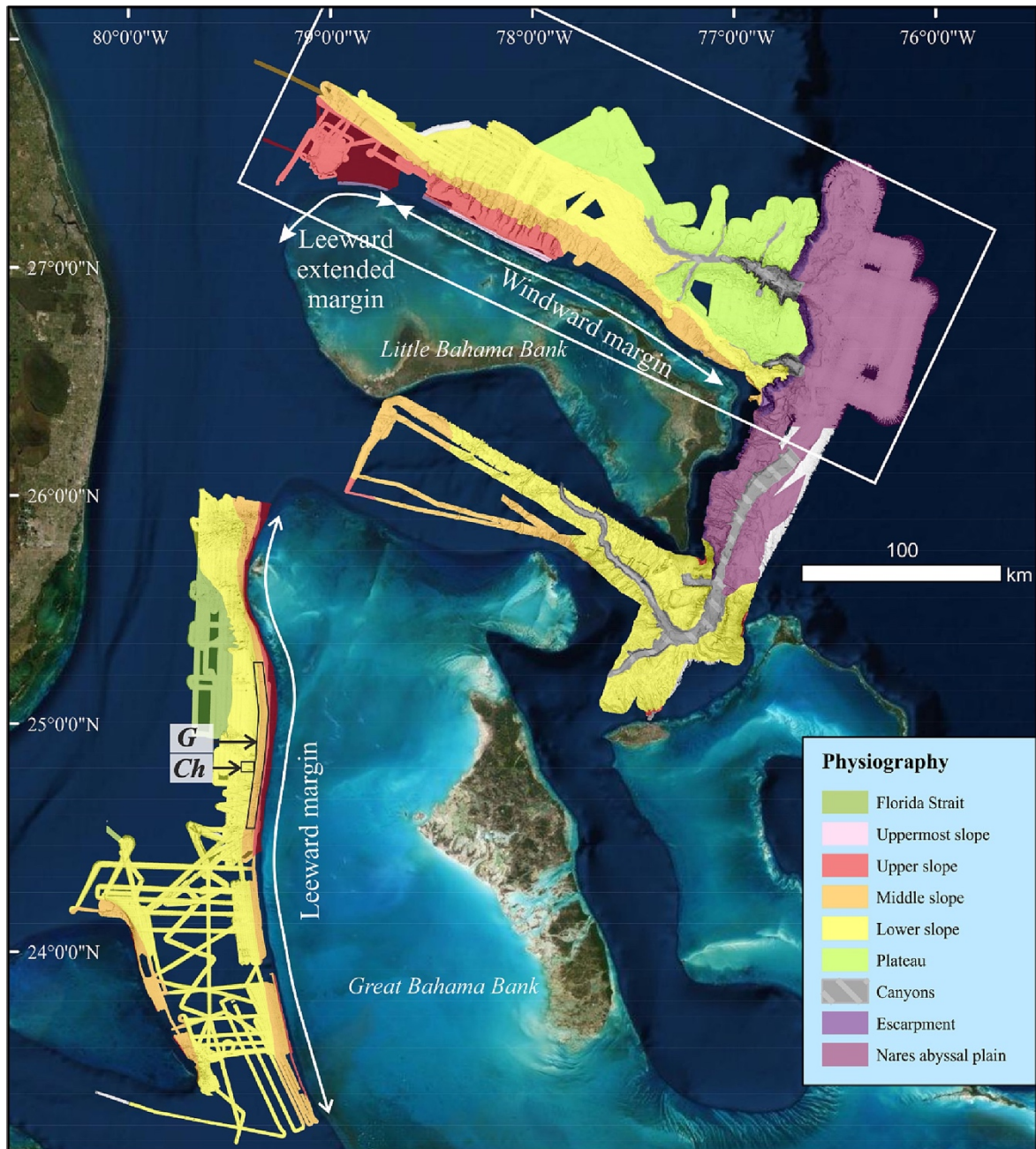


Fig. 3. Physiography of the Bahamian slopes and wind-related margins. White rectangle marks the location of the Little Bahama Bank slope detailed in Fig. 4. G: Gullies. Ch: Channel-levee system.

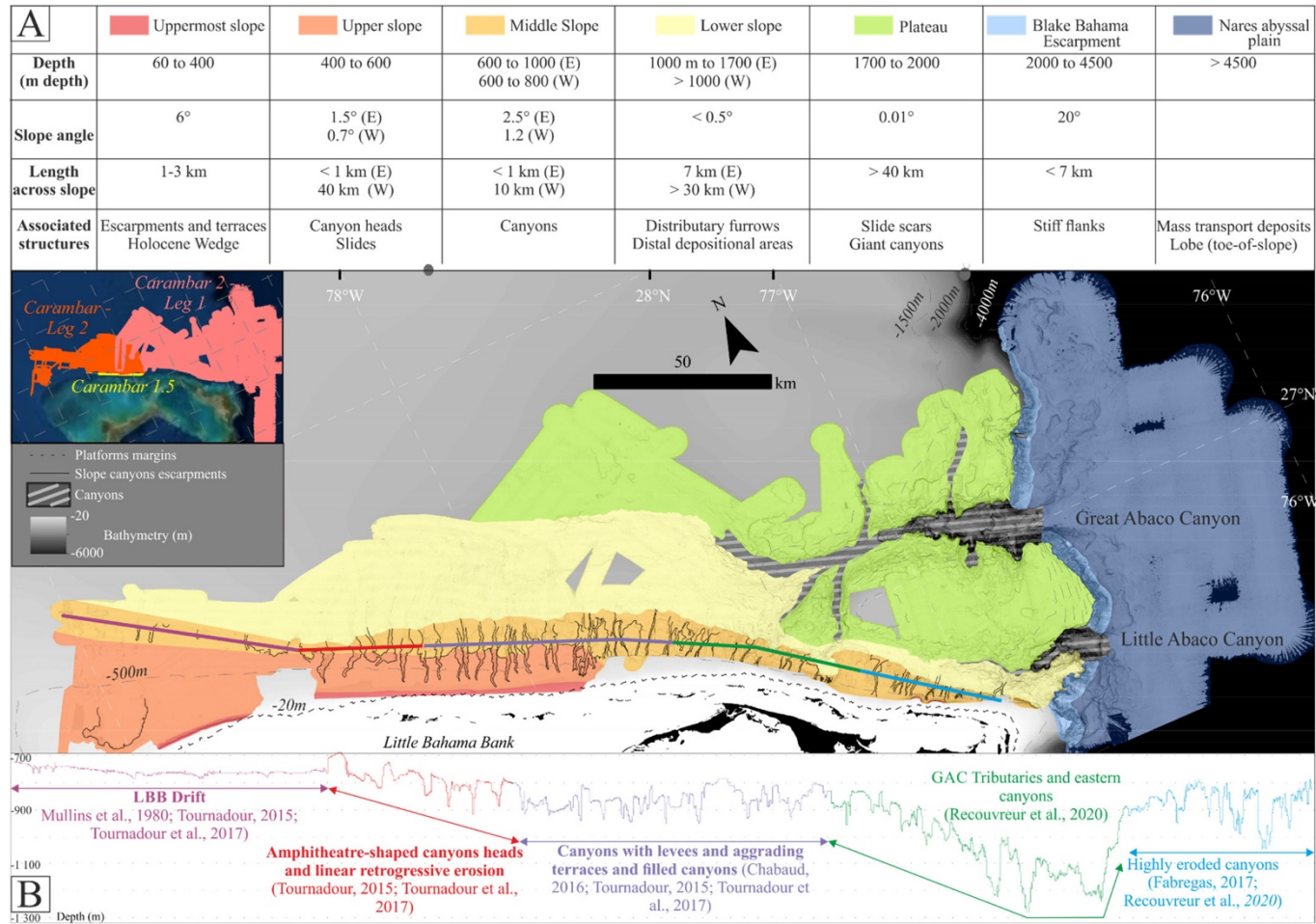


Fig. 4. (A) Morphological domains classified by water depth and (B) depth profile of the related physiographic domains observed along the northern slope of LBB (Mullins et al., 1980; Chabaud et al., 2015; Tournadour, 2015; Tournadour et al., 2015; Chabaud, 2016; Tournadour et al., 2017; Recouvreur et al., 2020).

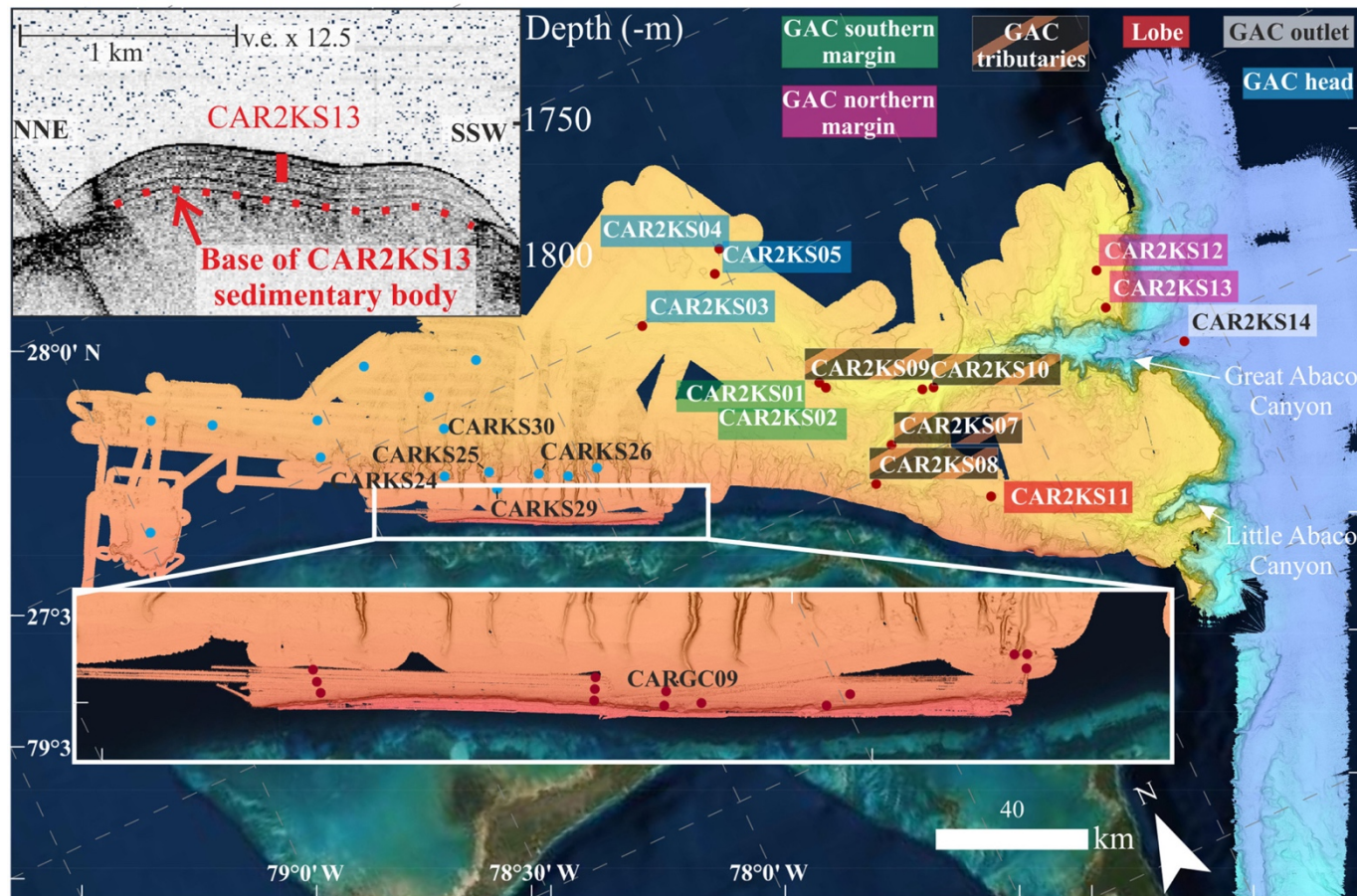


Fig. 5. Location map showing the location of sediment cores (red dots) used in this study (database detailed in Table 2). Cores analysed in earlier publications (Chabaud et al., 2015; Chabaud, 2016; Fauquembergue et al., 2018) that were incorporated in the analysis of sedimentation patterns on northern LBB slope are illustrated by blue dots, and cores mentioned in this study are labelled. Top left: VHR seismic profile showing the sedimentary context of core CAR2KS13 (Eastern part map).

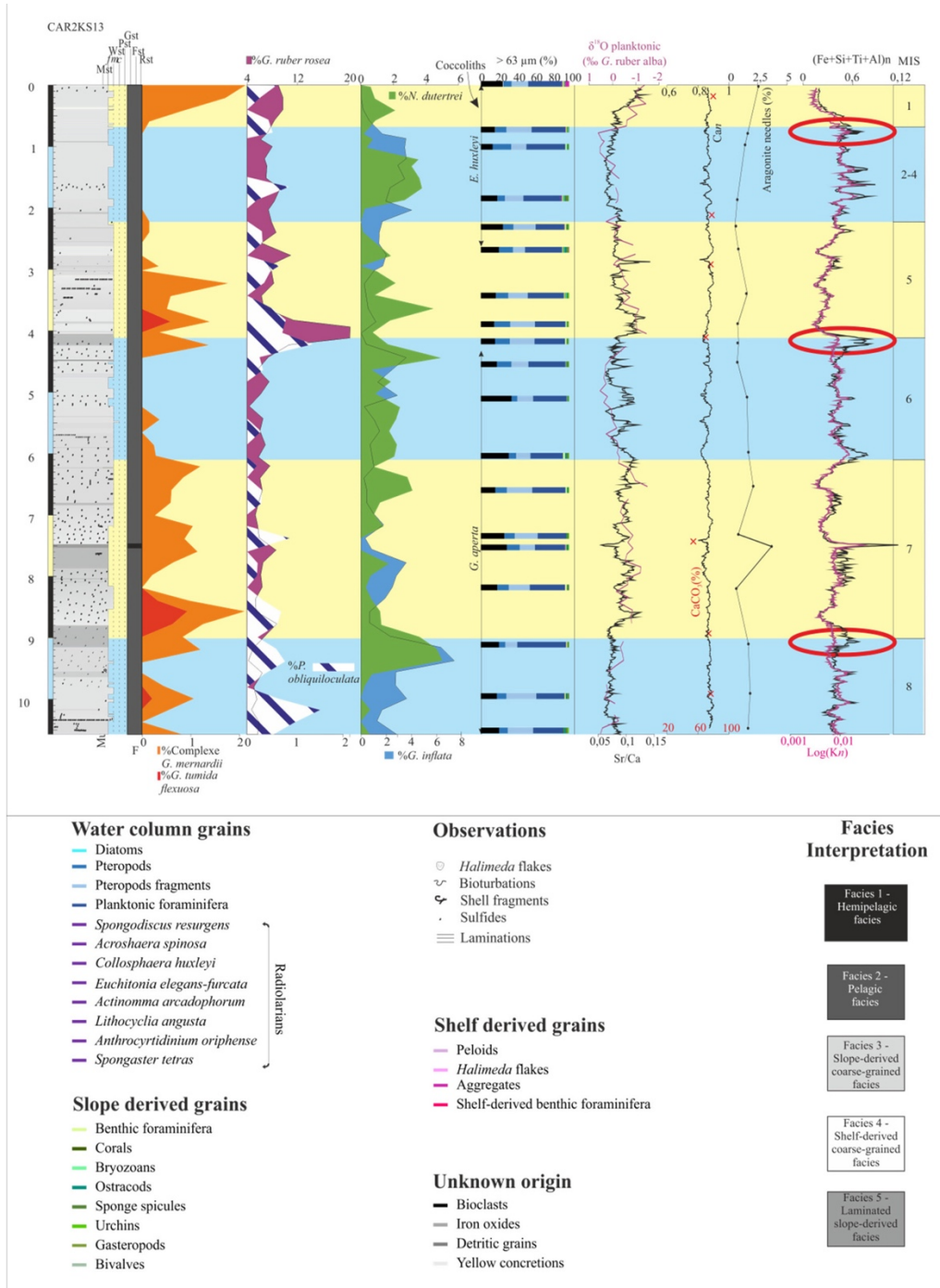


Fig. 6. Stratigraphy and sedimentological data for core CAR2KS13. Presented are detrital supply variation (Fe + Si + Ti + Al)n, potassium supply variation (Log Kn) and grain content. CaCO₃ content and proportion of aragonite needles estimated from samples. Red circles highlight the difference in variation between detrital and potassium supply. Sediment classification follows Dunham (1962). Stratigraphy uses MIS (Lisiecki and Raymo, 2005). F corresponds to the interpretative facies.

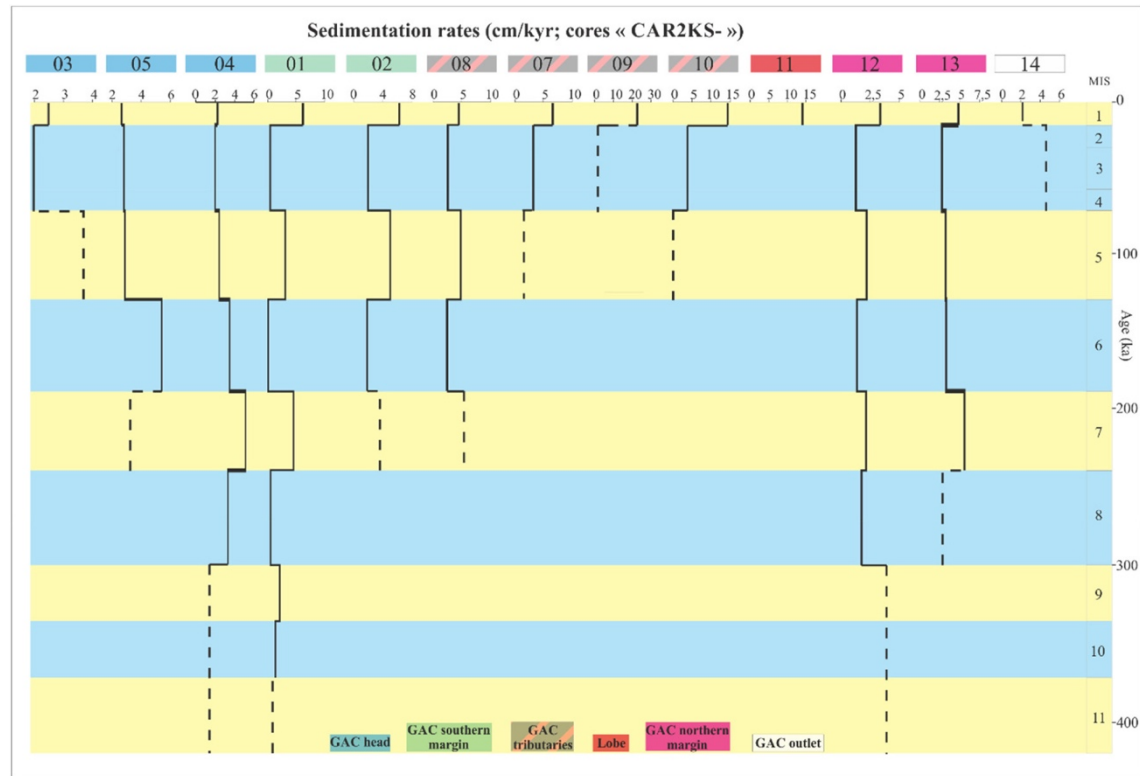


Fig. 7. Sedimentation rates by MIS obtained on LBB studied cores, from western to eastern areas. Yellow intervals represent interglacials and blue intervals glacials. MIS stratigraphy and ages shown on the right. MIS recorded at the base of the cores (dotted line) are assumed to be incomplete.

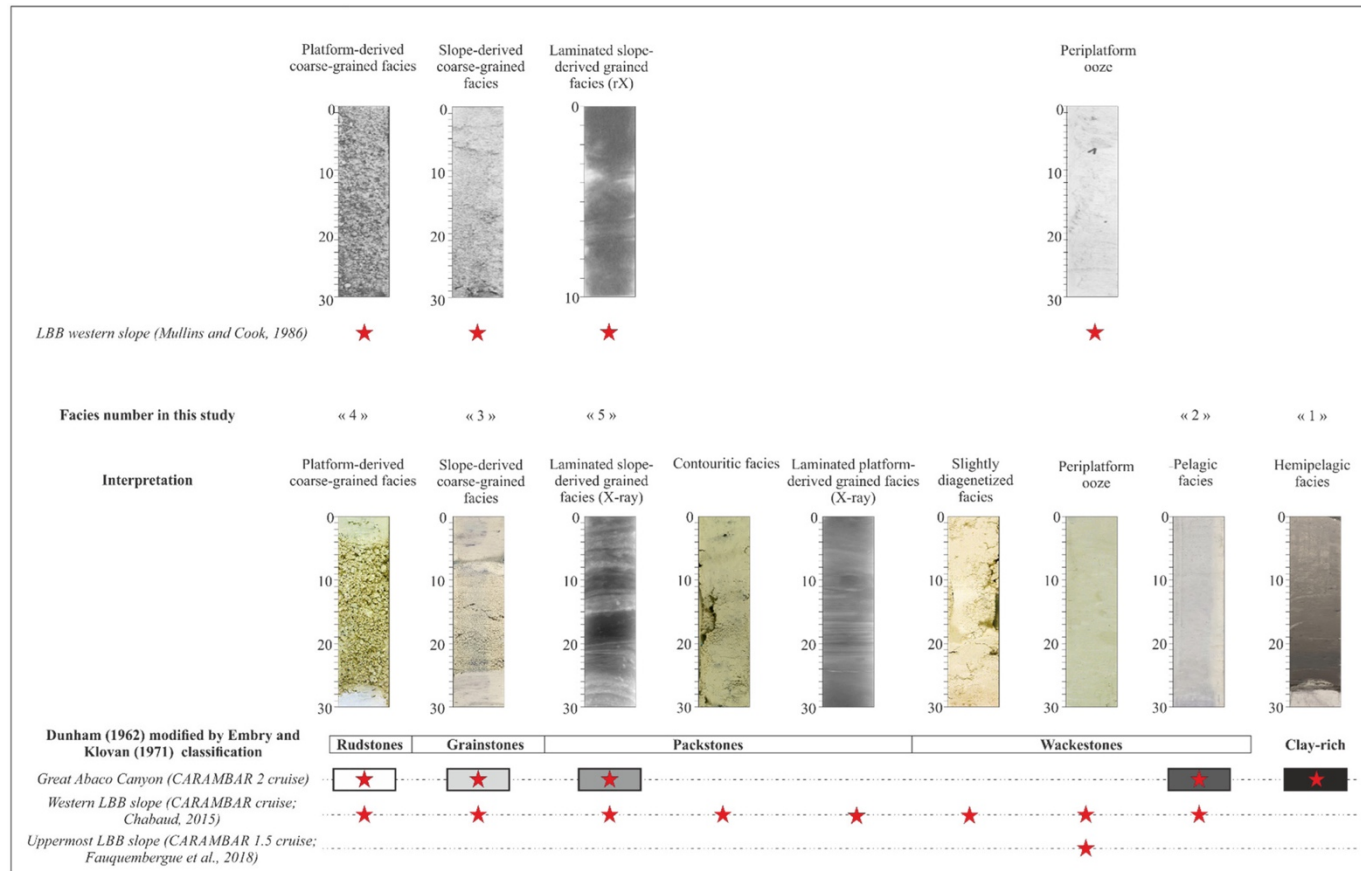


Fig. 8. Synthesis of facies observed along the northern LBB slope. Red stars allow to retrace the study area where each facies was recognized. Facies overview of Mullins and Cook (1986) and those defined on previous studies by the CARAMBAR project (Chabaud et al., 2015; Chabaud, 2016; Fauquembergue, 2018; Fauquembergue et al., 2018) are exposed, and the ones found in this study are defined as “Great Abaco Canyon (CARAMBAR 2 cruise)”. Colours associated to each facies on cores descriptions on Figs. 6, 9, 10 and 11 are shown behind the red stars of “Great Abaco Canyon (CARAMBAR 2 cruise)” (Embry and Klovan, 1970).

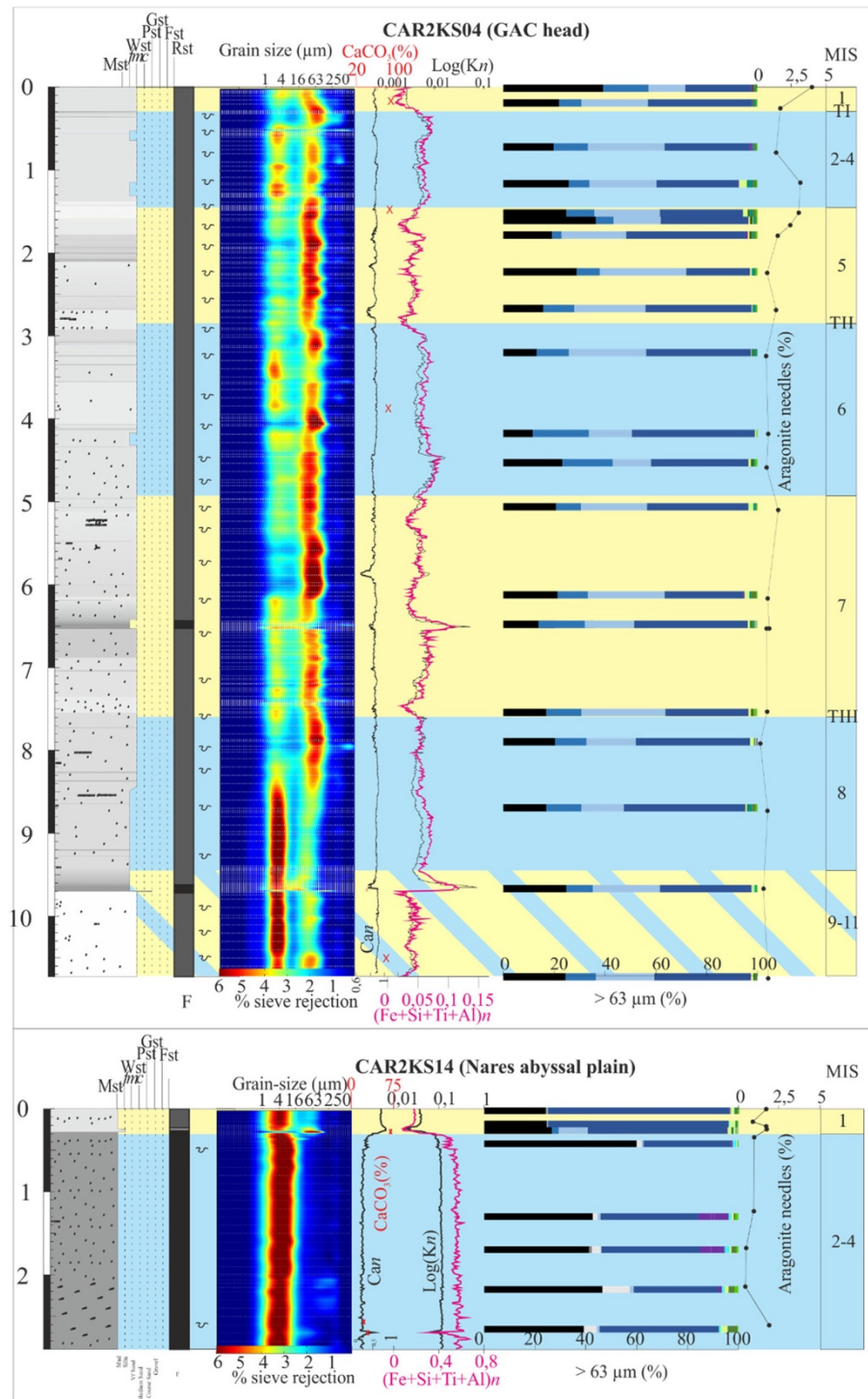


Fig. 9. Stratigraphy and sedimentological data collected for cores CAR2KS04 and CAR2KS14: grain-size distribution. Detrital supply ($\text{Fe} + \text{Si} + \text{Ti} + \text{Al}$)_n and potassium supply variation ($\text{Log } Kn$). Grain content (see legend in Fig. 6). CaCO_3 content and proportion of aragonite needles estimated from samples. Sediment classified according to Dunham (1962). Stratigraphy according to MIS (Lisiecki and Raymo, 2005). F corresponds to the interpretative facies (see legend).

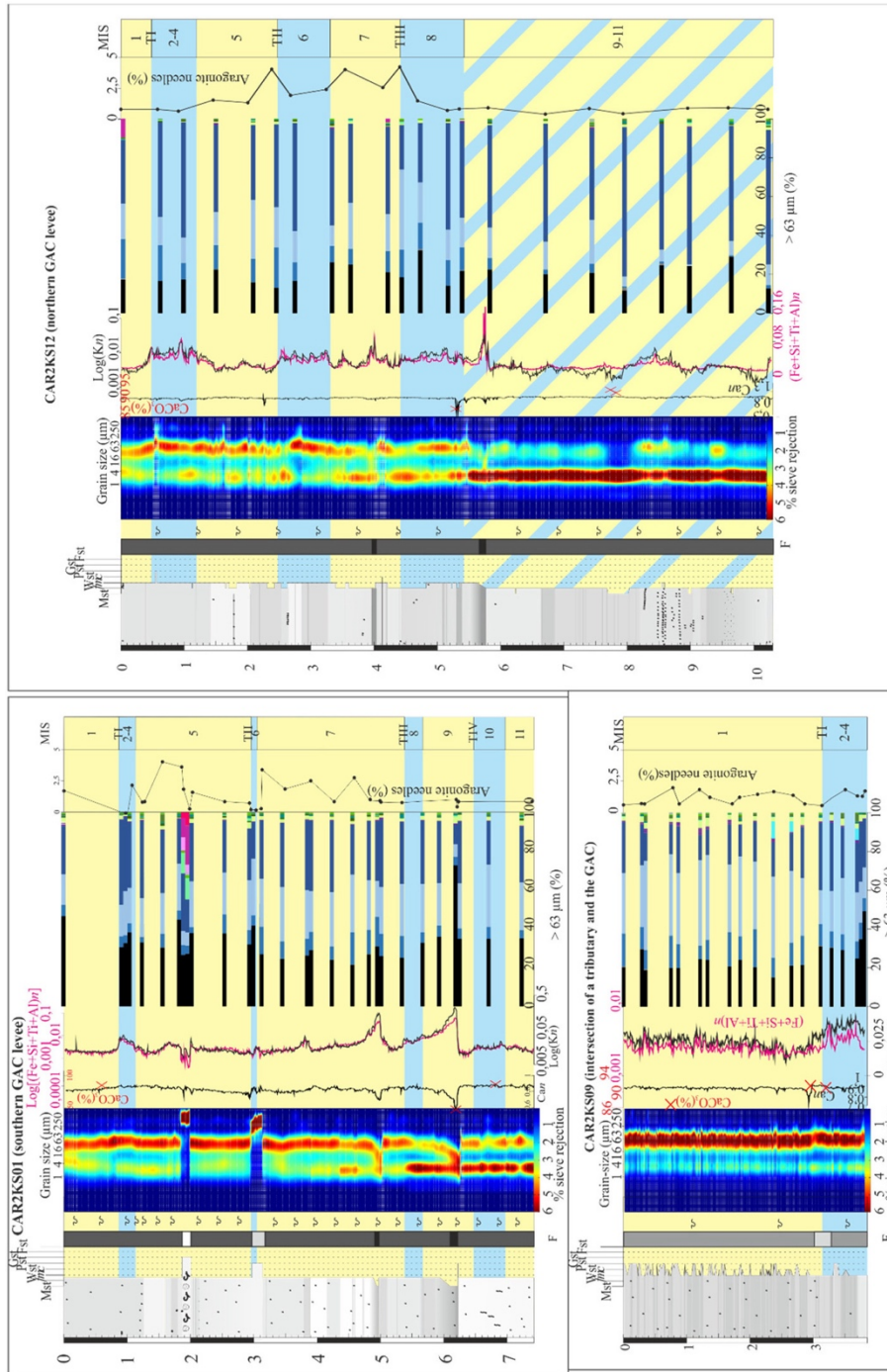


Fig. 10. Stratigraphy and sedimentological data for cores CAR2KS12, CAR2KS01 and CAR2KS09: grain-size distribution. Detrital supply (Fe + Si + Ti + Al) n and potassium supply variation (Log Kn). Grain content (see legend in Fig. 6). CaCO₃ content and proportion of aragonite needles estimated from samples. Sediments classified using Dunham (1962) and stratigraphy follows Marine Isotopic Stages (MIS; Lisiecki and Raymo, 2005). F corresponds to interpretative facies (see Fig. 6 for legend).

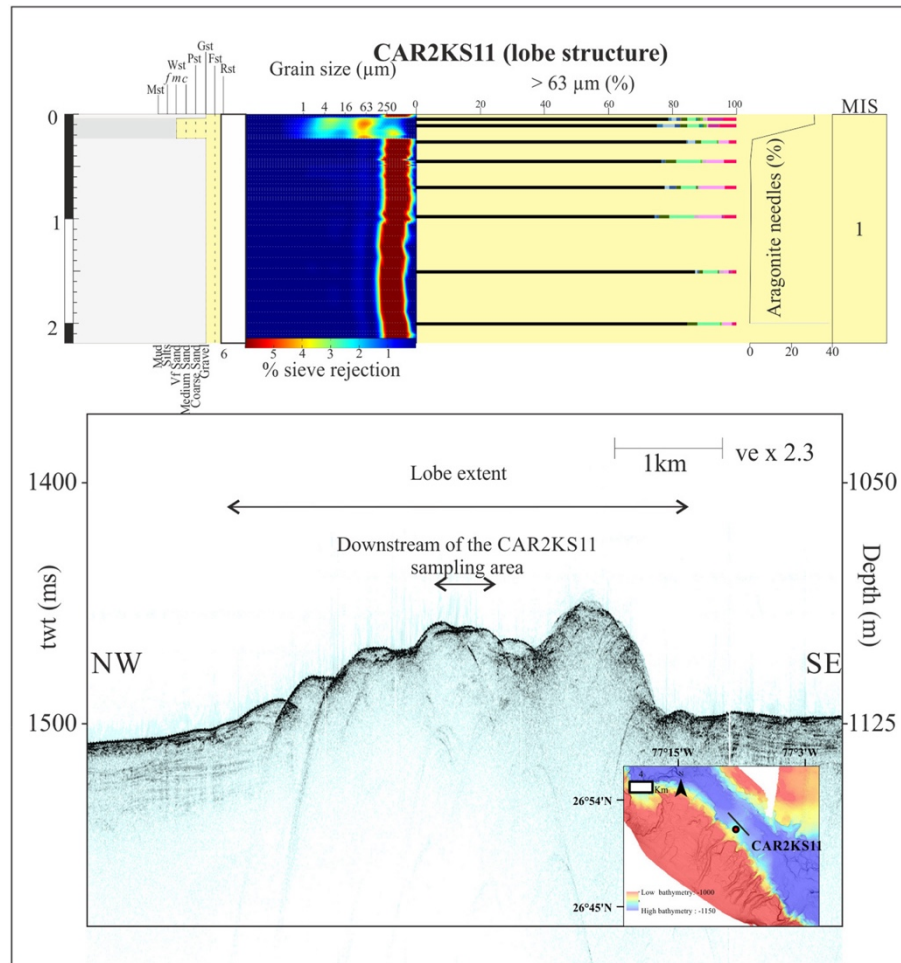


Fig. 11. Stratigraphy and sedimentological data for core CAR2KS11. Top figure: grain-size distribution. Grain content (see Fig. 6 for legend). Sediments classified using Dunham (1962) and stratigraphy follows Marine Isotopic Stages (MIS; Lisiecki and Raymo, 2005). CaCO_3 content and proportion of aragonite needles estimated from samples. F corresponds to interpretative facies (see Fig. 9 for legend). Lower caption: High resolution seismic profile across core location and water depth map; orange colour 1000 m water depth, purple colour: 1150 m water depth.

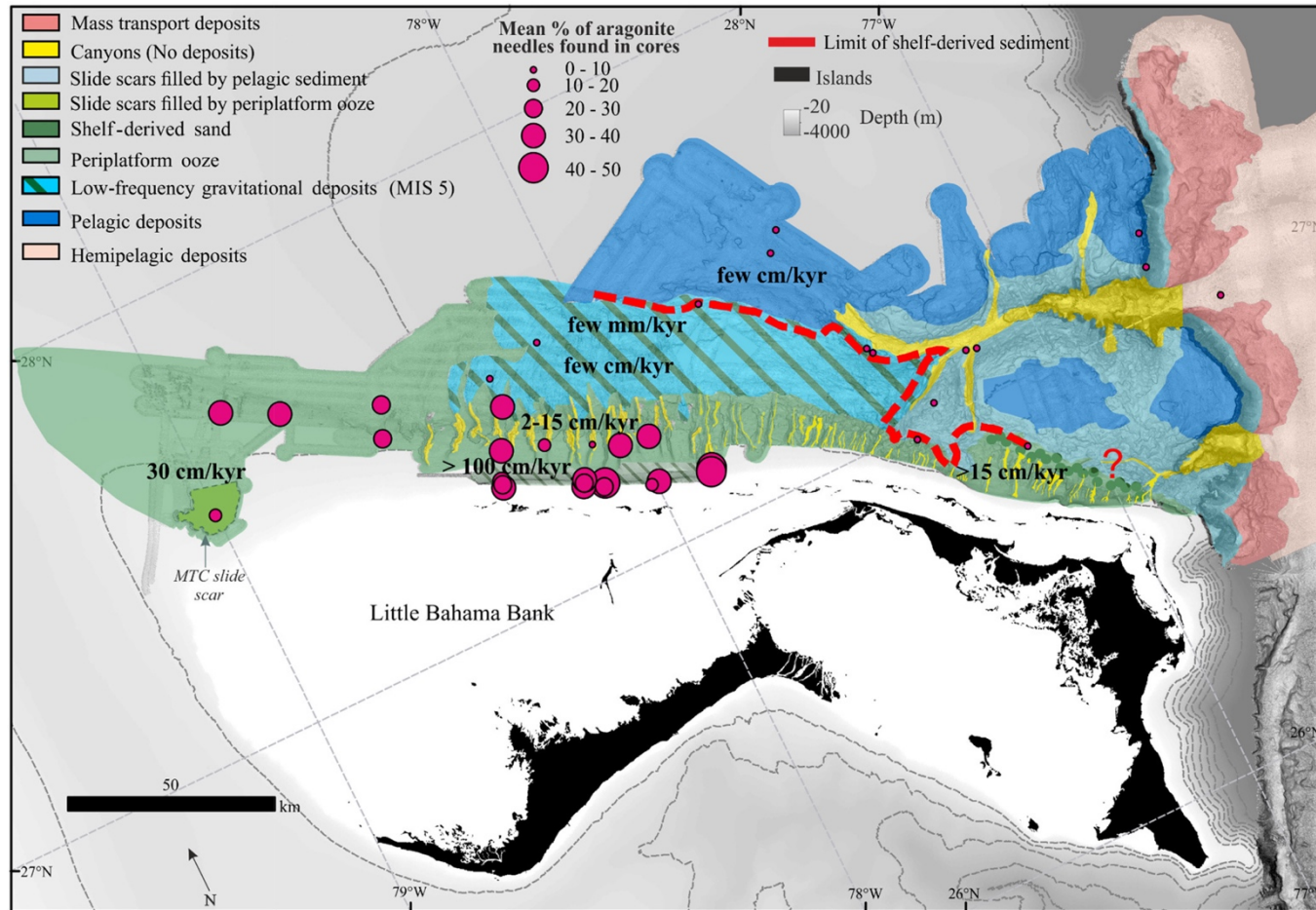


Fig. 12. Dominant Quaternary sedimentary processes along the northern slope of the LBB. Shown are: Dominant sediments, mean sedimentation rates and highstand shedding model limits (red dashed line).

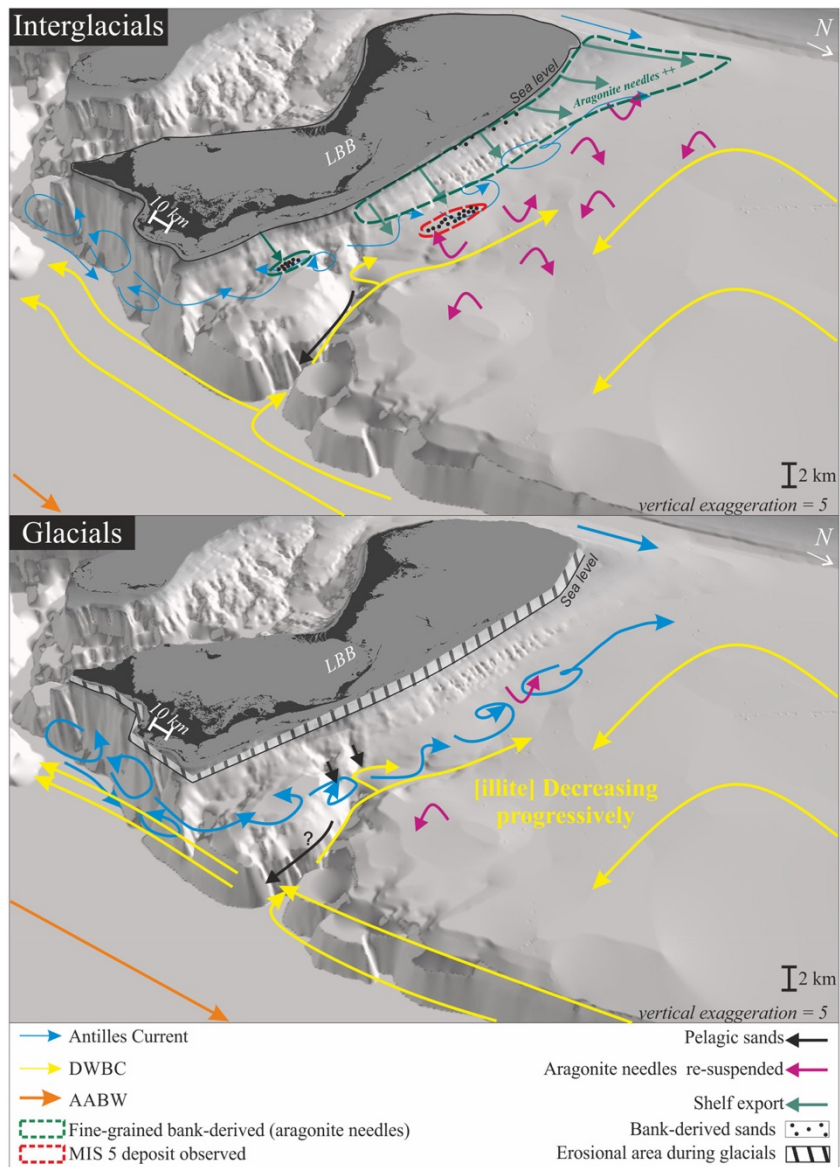


Fig. 13. Scheme of sediment export during glacial (lower panel) and interglacials (upper panel) along the northern LBB.

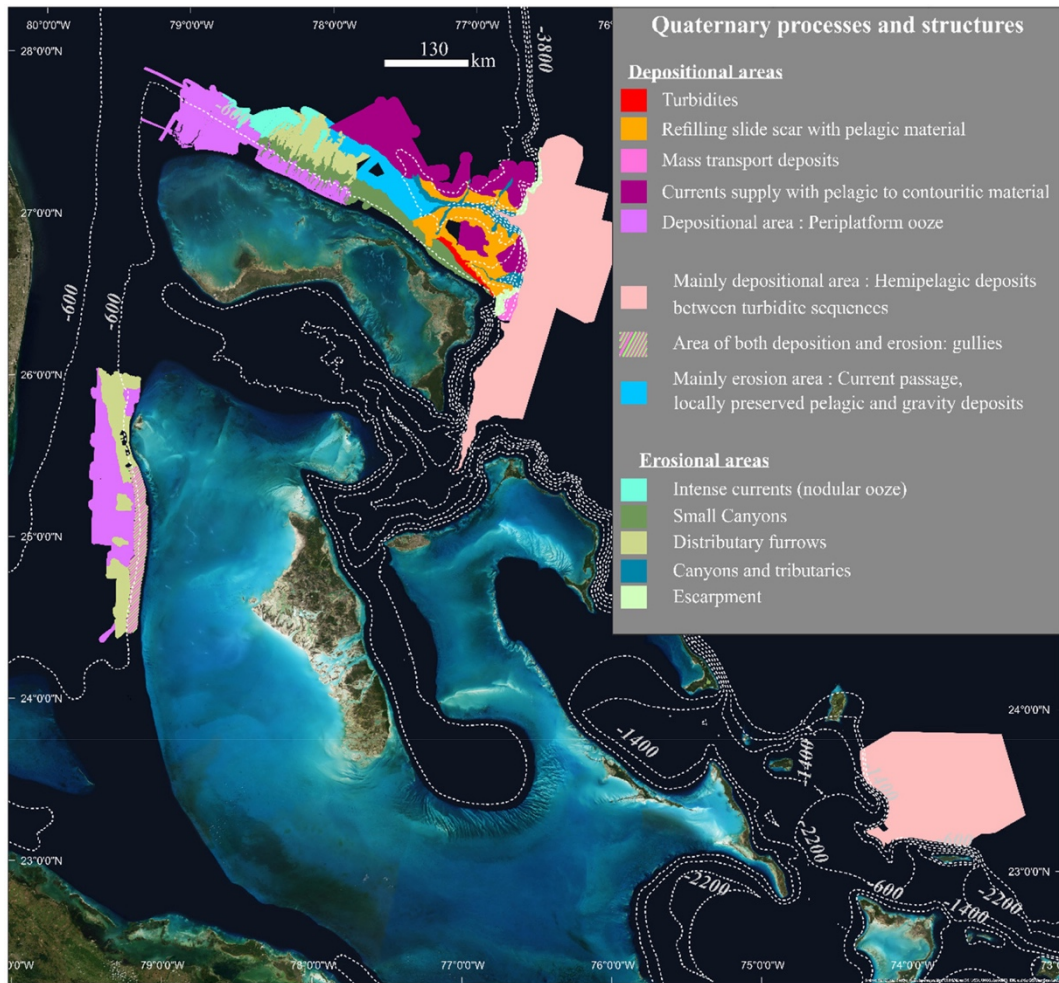


Fig. 14. : Map with sedimentation and erosion areas as identified along the Bahamian slopes together with the associated Quaternary sedimentation processes.

Table 1

Summary of different types of bathymetric and acoustic reflectivity data collected during the surveys.

Cruises	Data	Acquisition tool	Penetration \pm Resolution	Data acquired	Software
CARAMBAR 2 – Leg 1	VHR seismic	Chirp subbottom profiler (1,8–5,3 kHz)	$\sim 200 \text{ m} \pm 20 \text{ cm}$	3778 km	QC Subop
	Bathymetry Reflectivity	Kongsberg EM122 multibeam echosounder (12 kHz)	$\pm 50 \text{ m}$	15,784 km ²	Caraibes Sonarscope
CARAMBAR 1.5	VHR seismic	Knudsen Chirp 3260 (3.5 kHz)	$\sim 40 \text{ m} \pm 10 \text{ cm}$	1120 km	SounderSuite
	Bathymetry Reflectivity	Teledyne Reson Seabat 7125 multibeam echosounder	$\pm 5 \text{ m}$	150 km ²	Caraibes Caraibes
CARAMBAR	VHR seismic	Chirp subbottom profiler (1,8–5,3 kHz)	$\sim 200 \text{ m} \pm 20 \text{ cm}$	3154 km	MatLab
	Bathymetry Reflectivity	Kongsberg EM302 multibeam echosounder (30 kHz)	$\pm 20 \text{ m}$	4895 km ²	Caraibes Caraibes

Table 2

Little Bahama Bank cores lengths.

Core	Latitude (N)	Longitude (W)	Water depth (m)	Core length (m)
CAR2KS01	27°13.637	77°24.767	1383	7.42
CAR2KS02	27°12.713	77°24.222	1424	7.765
CAR2KS03	27°29.467	77°44.042	1287	3.67
CAR2KS04	27°34.165	77°29.581	1313	10.74
CAR2KS05	27°31.542	77°31.659	1378	8.675
CAR2KS07	27°02.663	77°19.235	1352	3.63
CAR2KS08	26°59.005	77°23.538	986	9.11
CAR2KS09	27°06.995	77°10.426	1957	3.855
CAR2KS10	27°07.396	77°11.939	1960	4.33
CAR2KS11	26°51.488	77°09.565	1090	2.19
CAR2KS12	27°11.714	76°42.517	1552	10.3
CAR2KS13	27°06.984	76°43.583	1766	10.58
CAR2KS14	26°58.935	76°35.538	4873	2.895

Table 3

Ages of sedimentary bodies sampled on northern LBB margin.

Core	Estimated sedimentary body age	Age
CAR2KS10	-0,29 Ma	
CAR2KS09	-0,32 Ma	
CAR2KS13	-0,48 Ma	
CAR2KS08	-0,54 Ma	Middle Pleistocene
CAR2KS07	-0,55 Ma	
CAR2KS04	-0,72 Ma	
CAR2KS02	-0,8 Ma	
CAR2KS05	-0,9 Ma	
CAR2KS01	-1 Ma	Lower Pleistocene
CAR2KS03	-1,4 Ma	
CAR2KS12	-2,3 Ma	

Table 4

Synthesis of different information available at deep current locations. MIS, location, lysocline water depth, and depth CCD since the MIS 10 in the Northeast Atlantic Ocean (Balsam, 1983; Keigwin et al., 1998a; Oppo et al., 2001; Yokoyama and Franz, 2002; Franz and Tiedemann, 2002; Heusser and Oppo, 2003; Meinen et al., 2004; Johns, 2011; Bořhm et al., 2015). Core numbers indicated when situated close to data location. AABW: Antarctic Bottom Water; BBOR = Blake Bahama Outer Ridge; WBUC: NADW: North Atlantic Deep Water; Western Boundary Undercurrent.

MIS	Deep current circulation	Lysocline depth (m)	CCD depth (m)
1	WBUC: 4763 m - 2000 m (BBOR)	4050–4350	Lower than 4980 ACD: 2000 (James and Choquette, 1983) or 4100 (Balsam, 1983; Droxler et al., 1988a)
2	AABW intensification (Muir Seamount)	Between 1780 and 2705	
3		3800	4650
4	AABW upwelling during cold events (C19. C20; BBOR)	3400	
5.2	AABW upwelling during cold events (C21. C22; BBOR)		4650
5	5.4 AABW upwelling during cold events (C23. C24. C25 and C26; BBOR)	3400	4650
	5.5 AABW upwelling during cold events (C27; BBOR)		Lower than 4980
	8.3 Top of AABW between 1800 m and 2000 m (BBOR)	shallower lysocline	
8	8.4 Top of AABW between 1800 m and 2000 m (BBOR)	shallower lysocline	
	8.5 (warm period) NADW: 2200 m – 3000 m (BBOR)		
	8.6 Top of AABW at 3000 m (BBOR)	shallower lysocline	
Termination IV	NADW lower limit reduced from 3000 m to 2200 m depth (BBOR)		
	9.1 (warm period) NADW: 1800–3000 m (BBOR)		
9	9.3 (warm period) NADW: 1800–3000 m (BBOR)		
10	10.2 NADW: 1150 m - 1800 m Top of AABW at 2200 m (BBOR)	shallower lysocline	